FCP Report No. 35

FATIGUE CRACK INITIATION AND GROWTH IN GRAY CAST IRON

by

James W. Fash
Department of Mechanical and Industrial Engineering

Fatigue properties of gray cast irons are related to the morphology of the free graphite phase. Deformation resulting in the initiation of fatigue cracks occurs at low stress levels due to the local stress concentration of the graphite flakes. Formation and growth of fatigue cracks during totally reversed strain control fatigue tests of a pearlitic gray iron has been monitored using a surface replicating procedure. Cracks initiate within the first 10% of specimen fatigue lives and the development and growth of multiple crack systems has been observed. A continually decreasing peak tensile load throughout fatigue tests is shown to relate closely to the developing crack systems and is not the result of cyclic softening. Results of fatigue tests of two ferritic gray irons with differing eutectic cell sizes are also reported. Observation of decreasing peak tensile loads infers the accumulation of damage as the development of cracks. The rate of load drop is found to increase with increasing eutectic cell diameter.

A Report of the
FRACTURE CONTROL PROGRAM
College of Engineering, University of Illinois
Urbana, Illinois 61801

October, 1980

ABSTRACT

Fatigue properties of gray cast irons are related to the morphology of the free graphite phase. Deformation resulting in the initiation of fatigue cracks occurs at low stress levels due to the local stress concentration of the graphite flakes. Formation and growth of fatigue cracks during totally reversed strain control fatigue tests of a pearlitic gray iron has been monitored using a surface replicating procedure. Cracks initiate within the first 10% of specimen fatigue lives and the development and growth of multiple crack systems has been observed. A continually decreasing peak tensile load throughout fatigue tests is shown to relate closely to the developing crack systems and is not the result of cyclic softening. Results of fatigue tests of two ferritic gray irons with differing eutectic cell sizes are also reported. Observation of decreasing peak tensile loads infers the accumulation of damage as the development of cracks. The rate of load drop is found to increase with increasing eutectic cell diameter.

ACKNOWLEDGMENTS

This investigation was conducted in the Materials Engineering Research Laboratory, University of Illinois, Urbana.

Mrs. Darlene Mathine is gratefully acknowledge for typing the manuscript.

TABLE OF CONTENTS

LIST OF TABLES

LIST OF FIGURES

I. INTRODUCTION

Prior investigations into the stress-strain behavior and fatigue resistance of cast irons have indicated that the morphology of the free graphite phase governs the material response. In an experiment to model the anelastic response of cast materials, Thum and Ude [1] tested steel plates with varying notch geometries. As the notch severity increased, the tangent modulus decreased, indicating that increasing notch severity increases the damage accumulated at a given load. Cast irons show this trend. In nodular iron the stress concentration factor of the spherical graphite is less than that for a graphite flake found in gray iron. It follows that, in general, nodular iron is superior in fatigue.

In a series of experiments [2-5] Gilbert observed deformation of cast irons in tension and compression. Upon tensile loading, the free graphite was found to either crack or debond at the matrix interface. Voids were created when yielding occurred in the matrix material, which occurred at low overall stress levels due to the large stress concentrations at the free graphite. Cracks initiated in these highly stressed regions.

Ohira and Ikawa [6], Starkey and Irving [7], and Testin [8] have observed crack formation and growth in nodular iron. During fatigue, cracks initiate from nodules throughout the material and grow in a linking process with other nodules and crack systems. Casting imperfections such as inclusions, porosities, and poorly formed nodules often have a more severe notch effect than spherical nodules and have been observed to initiate failure. Starkey and Irving monitored the growth of fatigue cracks in nodular iron and found cracks very early in the life of specimens. They reported 95% of the specimen lifetime being spent in crack growth.

Similar observations of crack initiation and growth have been made in gray cast iron. During tensile loading, cracking and debonding of the brittle free graphite phase causes void formation. Voids and subsequently cracks initiate first at flakes most normally oriented to the loading direction, but are observed to form from randomly oriented flakes at higher loads. Voids and cracks formed during tensile loading are closed when yielding occurs in compression. Compressive loads are more readily accommodated by the free graphite which causes gray iron to have a higher tangent modulus and greater strength in compression than in tension. To account for the anelastic response of gray iron, Gilbert [9] proposed a model which separates strain into four components: elastic and plastic deformation of the matrix and recoverable and permanent deformation due to void formation.

Ikawa and Ohira [6] and Mitchell [10] have investigated the effects of matrix microstructure and the size and shape of the free graphite on fatigue resistance of cast irons. Decreasing the notch severity of the free graphite phase improved the fatigue behavior, which in gray iron is accomplished by decreasing the graphite flake size. Increasing the matrix hardness was found to have a greater effect upon improving fatigue behavior than changing the matrix microstructure. Fatigue data reported by Mitchell (Fig. 1) shows the effects of changing matrix microstructure and hardness. Compilation of fatigue data readily available for gray iron is shown in Fig. 2. Variability in the fatigue performance is shown by the relatively large scatter of data. It is not well understood which major microstructural or chemical variables most significantly control which irons fall at the high end of the scatter (best fatigue performance).

Cast iron is an internally notched material and an understanding of the microdiscontinuities requires a brief discussion of the solidification process.

Upon cooling the free graphite precipitates from the molten alloy. Nucleation sites occur throughout the material with the formation of the graphite and solidification occurring in approximately spherical fronts. Structure of the bars during the solidification process are shown in Fig. 3. The spherical colonies formed are called eutectic cells and the structure of the weak, free graphite within the cell is continuous through the diameter as shown in Fig. 4 [11]. A more detailed discussion of the solidification process can be found in reference [12]. Upon loading, the free graphite cracks forming discontinuities equal in size to the eutectic cell diameter.

Mitchell [13] used macroparametric strain life concepts to model the fatigue of cast materials. This approach employs strain life concepts used to predict crack initiation lifetimes, incorporates a Neuber analysis developed to accommodate geometrical notches in wrought materials [14] and modified for fatigue, and takes into account the size of the discontinuities present. Gray iron is modeled as a high silicon, wrought steel with surface notches equal in size to the eutectic cell diameter.

Reasonable life predictions for constant amplitude loading were made with this model. At shorter lives (less than 10^3 cycles) nonconservative predictions were made.

Formation of cracks early in the fatigue life, observed by many of the authors previously cited, indicates that a crack initiation model might not adequately describe the continuous accumulation of damage in cast materials under variable amplitude loading. For improved life predictions of cast components a better understanding of the fatigue processes and accumulation of damage is required. In this investigation the formation and growth of fatigue cracks in a pearlitic gray cast iron has been observed by a replicating procedure used to record the entire specimen surface at intervals

throughout the fatigue lifetime. Initiation of cracks and the development of multiple cracks systems were observed very early in the life of specimens with most of the life being spent in crack growth. As damage accrues in the material from each loading cycle, the compliance of the specimen changes. In strain cycle fatigue tests this is shown by a decrease in the load obtained at the tensile strain peak through fatigue tests. Load drop has been monitored and is found to correlate closely with crack growth. Relative differences in the rate of crack development at different strain amplitudes was observed.

Results of fatigue tests of two ferritic gray irons with different eutectic cell sizes are presented. Load drop during fatigue tests was observed, and it is suggested that the accumulation of damage in the material is related to the drop in the peak tensile load at successive cycles during the test. It is observed that for a given strain amplitude, load drop occurs at the fastest rate for the iron with the largest eutectic cell diameter, indicating that the notch effect of the free graphite in the eutectic cell increases in severity with an increasing cell size.

II. MATERIAL DESCRIPTION

Materials tested in this investigation were provided by Deere and Co. Test bars, 36 mm in diameter and 200 mm long, were cast in green sand molds to produce the pearlitic gray iron. Matrix microstructure and flake structure, classified by ASTM A247 [14] as ∿60% type A, ∿40% type D, size 4 are shown in Fig. 5. Test bars of the ferritic irons were cast in diameters of 36 mm and 50 mm to produce different eutectic cell structures. Flake structures (Fig. 6) were determined to be ∿50% type A, ∿50% type D, size 5 for the iron designated "A", and ∿50% type B, ∿50% type D, size 2 for the iron designated "B".

Steads reagent was used to preferentially etch the materials to allow determination of the eutectic cell size. The average eutectic cell size of the pearlitic iron was 0.14 mm. Eutectic cell diameters of the A and B irons were determined to be 0.52 mm and 0.75 mm respectively and are shown in Fig. 7.

Materials chemistries for the three irons are given in Table 1, and mechanical properties are given in Table 2.

III. TESTING PROGRAM

Specimens were machined to the dimensions given in Fig. 8 from the rough cast test bars. All tests were performed on a 20 kip MTS materials test system interfaced to a multiuser digital computer in the Materials Engineering Research Laboratory at the University of Illinois. Monotonic and fatigue tests were software controlled. Stress-strain data was digitized and stored on floppy disks. Tests for crack growth observations were performed using manual analog control but hysteresis response was recorded digitally using software controlled data acquisition.

A. Monotonic Tests

Monotonic tensile and compressive stress-strain behavior for the three irons (Figs. 9-11) indicate the anelastic response and asymmetry of the loading curves which is characteristic of cast irons. Lack of an elastic region of response is caused by damage (plastic yielding), which occurs at low stress levels in the matrix material because of the stress concentration of the free graphite phase. Compressive loads can be accommodated by the graphite flakes but voids form during tensile loading, causing the asymmetry between compressive and tensile curves. The monotonic tensile strength increases as eutectic cell size decreases (Fig. 12).

B. Fatigue Tests

Constant amplitude, totally reversed, strain control low cycle fatigue tests were performed at five different strain amplitudes for each iron. At least three specimens were tested at each amplitude. Hysteresis

loops were digitally recorded at every power of two cycles. Representative hysteresis response is shown in Figs. 13-21 for the three irons. Stable response is never realized as the peak tensile load drops off continuously. For this reason a cyclic stress-strain curve is not presented. Strain-life data is plotted in Fig. 22 for the three irons. The pearlitic iron, with the smallest eutectic cell, exhibited the best fatigue behavior and the B iron, with the largest eutectic cell diameter, performed the poorest (Fig. 23). Raw fatigue data is given in Appendix A.

Failure was recorded at 90% load drop from the initial maximum tensile load. As the crack system resulting in failure develops, geometrical factors become important. Loading conditions gradually change from axial loading to axial loading combined with bending as the crack system grows causing some variation in fatigue lives which can be explained by the location of the strain transducer in relationship to the developing crack system. If the major crack system develops between the mounting points of the strain extensometer, the load necessary to achieve the control strain is considerably less than the load that would be required if the crack were developing on the side of the specimen opposite the strain extensometer. Observations at about 85% of the specimen life, indicated that the load required to produce a given strain on the side of the specimen opposite the developing crack system was about 50% greater than that required when the strain transducer was mounted over the crack. This effect only occurs when the crack size has become large compared to the specimen cross section.

C. Crack Observations

Crack formation and growth was monitored in the pearlitic gray iron. A replicating procedure using standard metallographic acetyl cellulose film

was used to record the surface of specimens during fatigue. By softening the film with acetone and placing it around the gauge section of the specimen, a "cast" of the surface is obtained. Several techniques were attempted to observe the details of the replicas including SEM observation incorporated with evaporation or sputtering of conductive films. Observation of the replicas was accomplished using an optical microscope by illuminating through the replica.

Crack growth data was obtained by taking replicas at approximately every 10% of the expected life or at successive drops in load of four percent from the initial maximum tensile load. The replicating procedure allows qualitative observation of the amount and extent of crack development as well as quantitative observation of the crack system which grows to failure. Details of the replicating procedure and raw crack data are given in Appendix B and discussed in detail in the next section.

IV. RESULTS AND DISCUSSION

A. Qualitative Observations

Crack formation and growth have been observed by recording replicas of the surface at intervals in the life of fatigue specimens. Deformation occurs in the matrix material upon the first tensile loading and in critically oriented graphite structures, cracking or debonding from the matrix causes crack-like void formation. Cracks initiated at microdiscontinuities grow in a complex process consisting of crack propagation through the matrix material and incremental crack extension from the linking of crack systems. Crack arrest via a type of crack-tip blunting has been observed when cracks link with flake structures oriented parallel to the loading axis or with hemispherical surface discontinuities.

At large strain amplitudes ($\Delta\varepsilon/2 = 0.003$) cracks have been found within the first four percent of the specimen life. Microdiscontinuities with the largest stress concentrations initiate cracks first, but damage, as evidenced by the formation of cracks, occurs throughout the material. Damage accrues over the entire specimen surface and many cracks of similar magnitude are growing through the duration of the test. Near failure, several cracks have grown to two millimeters in length and failure occurs by the linking of some of these crack systems. Tests performed at small strain amplitudes ($\Delta\varepsilon/2 = 0.001$) show initiated cracks within the first ten percent of the specimen life. Fewer major crack systems developed at this amplitude but small cracks are found throughout the specimen at intermediate lives. Near failure, very few crack systems have developed to two millimeters in length.

B. Quantitative Observations

Development of the crack system resulting in failure has been measured from the surface replicas. At a given life the crack length, a, was taken as the length of the largest portion of the failure crack system distinguishable on the surface. When two or more crack systems were well developed and near joining, the sum of their lengths was considered as the crack length at the particular life. The initial flaw size was taken as the eutectic cell diameter.

Crack growth versus applied cycles data (Fig. 24) for the pearlitic gray iron indicates that most of the specimen life is spent growing a crack to a length of one to two millimeters. Once a crack reaches this length, growth occurs rapidly, resulting in failure in a relatively few number of cycles. Normalized cycles (cycles/cycles to failure) versus crack length, shown in Fig. 25, indicates that as strain amplitude increases, the rate of growth of small cracks increases. The development and growth of crack systems is related to the damage accumulation. As strain increases, larger matrix deformation and faster crack development are observed indicating increasing damage rate with increasing strain amplitude.

At small strains, only flakes most normally oriented to the loading axis initiate cracks, which results in only a few cracks systems developing extensively. At larger strains cracks will initiate at flake orientations increasingly oblique to the loading axis as well as those normally oriented to the loading direction. This results in an increasing number of crack systems at higher strains.

During strain cycle fatigue tests the specimen compliance increases throughout the test due to the accumulation of damage. This results in a continuous drop in the maximum tensile stress reached on each successive cycle

during the test. Tucker and Olberts [16] reported cyclic softening of cast iron specimens at approximately 45% of the life. Cycle changes would be expected to stabilize early in the life, and it is suspected that the load drop was due to crack formation (damage accumulation), not cyclic softening. Figure 25 shows stress versus normalized cycles for the specimens in which crack growth was monitored. A continual decrease in the peak tensile stress was observed. Load drop trends vary with strain amplitude in a manner consistent with the crack growth trends, i.e. at small strain amplitudes the load drop rate, related to the slope of the stress versus cycles data, is less than at large amplitudes.

Load drop and crack growth curves relate closely and are consistent throughout except for the specimen monitored at $\Delta\varepsilon/2 = 0.002$. The specimen life of this test was approximately an order of magnitude less than the average life of other tests at this amplitude and a sizable surface discontinuity (Fig. B2) was the sight of crack initiation.

C. Cyclic Response of Ferritic Irons

Hysteresis response for the two ferritic gray irons was recorded throughout the fatigue tests using computer controlled data acquisition. Cyclic hardening occurred in the first few cycles but after ten cycles no further hardening was observed. Representative load drop curves at four strain amplitudes are shown in Fig. 26 for the A and B irons. Load drop for a given strain amplitude is very consistent. The rate of load drop increased with increasing strain amplitude. Observations of the gauge section surface of ferritic iron specimens after fatigue testing indicate the formation and development of multiple crack systems similar to those

physically measured in the pearlitic iron. From this, the rate of damage accumulation in the form of crack systems can be inferred from the load drop curves. Slope of the load drop curves at two strain amplitudes for the three irons (Fig. 27) indicate increasing damage rate with increasing strain amplitude ($m_1 > \ell_1$; $m_2 > \ell_2$; $m_3 > \ell_3$). At a given strain amplitude the pearlitic iron had the slowest damage rate ($\ell_1 > \ell_2 > \ell_3$; $m_1 > m_2 > m_3$). Damage rate increased with increasing eutectic cell size which can be ascribed to the more severe notch effect of larger internal discontinuities.

V. CONCLUSIONS

Accumulation of fatigue damage, measured as the formation and growth of cracks, has been monitored in a pearlitic gray cast iron. Crack initiation occurred very early in fatigue specimens with observations of up to 96% of the life being spent in crack growth. Multiple crack formation and development indicates the accumulation of damage throughout the specimen. Continuous load drop phenomenon observed in strain controlled fatigue tests has been shown to relate closely with the development of crack systems and is not due to cyclic softening. This load drop phenomena is directly related to damage rate (crack development) which was found to increase with increasing strain amplitude for a given material. Comparing materials at a given strain amplitude, load drop occurs at a faster rate with increasing eutectic cell diameter. Techniques for improved life predictions of cast components during variable amplitude fatigue loading should result from a better understanding of the fatigue processes and damage accumulation in these materials.

REFERENCES

1. Thum, A. and Ude, H., "Die Elastizität und die Sahwingungsfestigkeit des Gusseisens," Die Giesserei, Vol. 16 (1929) pp. 547-556.

2. Gilbert, G. N. J., "Factors Relating to the Stress-Strain Properties of Cast Iron," J. of the British Cast Iron Research Association, Vol. 6 (1957) pp. 546-588.

3. Gilbert, G. N. J., "An Evaluation of the Stress-Strain Properties of Flake Cast Iron in Tension and Compression," J. of the British Cast Iron Research Association, Vol. 7 (1959) pp. 745-789.

4. Gilbert, G. N. J., "Variation of Microstructure of a Flake Graphite Cast Iron after Stressing in Tension and Compression," J. of the British Cast Iron Research Association, Vol. 12 (1964) pp. 31-47.

5. Gilbert, G. N. J., "The Stress-Strain Properties of Nodular Cast Irons in Tension and Compression," J. of the British Cast Iron Research Association, Vol. 12 (1964) pp. 547-556.

6. Ikawa, K. and Ohira, G., "Fatigue Properties of Cast Iron in Relation to Graphite Structure," American Foundry Society, Cast Metals Research Journal, Vol. 3 (1967) pp. 11-21.

7. Starkey, M. S. and Irving, P. E., "The Influence of Microstructure on Fatigue Crack Initiation in Spheroidal Graphite Cast Irons," GKN Technical Report, GKN Group Technological Centre, Wolverhampton, England.

8. Testin, R. A., "Characterization of the Cyclic Deformation and Fracture Behavior of Nodular Cast Iron," T&AM Report No. 371, Department of Theoretical and Applied Mechanics, University of Illinois, Urbana, Illinois (1973).

9. Gilbert, G. N. J., "The Components of Strain Due to Deformation of the Matrix and Due to Volume Changes in a Flake Graphite Cast Iron under Uniaxial Stress," J. of the British Cast Iron Research Association, Vol. 11 (1963) pp. 512-524.

10. Mitchell, M. R., "Effects of Graphite Morphology, Matrix Hardness, and Structure on the Fatigue Resistance of Gray Cast Iron," Society of Automotive Engineers, Inc., Report No. 750198 (1975).

11. Oldfield, W., "The Solidification of Hypo-Eutectic Gray Cast Iron," J. of the British Cast Iron Research Association, Vol. 8, No. 2, March (1960) pp. 177-192.

12. Heine, Loper, and Rosenthal, Principle of Metal Casting, Second Edition, McGraw-Hill Book Company (1967) pp. 575-587.

13. Mitchell, M. R., "A Unified Predictive Technique for the Fatigue Resistance of Cast-Ferrous Based Metals and High Hardness Wrought Steels," T&AM Report No. 412, Department of Theoretical & Applied Mechanics, University of Illinois, Urbana, Illinois (1976).

14. Topper, T. H., Wetzel, R. M., and Morrow, JoDean, "Neuber's Rules Applied to Fatigue of Notched Specimens," J. of Materials, Vol. 4, No. 1, March (1969) pp. 200-209.

15. "Method of Evaluating the Microstructure of Graphite in Iron Castings," ASTM Designation: A247, Plate I (Graphite Form Types), Plate II (Graphite Flake Type Chart), and Plate III (Graphite Size), American Society for Testing and Materials, 1916 Race Street, Philadelphia, Pennsylvania 19103.

16. Tucker, L. E. and Olberts, D. R., "Fatigue Properties of Gray Cast Iron," Society of Automotive Engineers, Inc., Report No. 690471 (1969).

TABLE 1. MATERIAL CHEMISTRY

	C	Si	Mn	S	P	Ti	Ni	Cr	Mo	Cu	Sn
Pearlitic Iron	3.30	2.20	.44	.02	.01	.01	.06	.03	.01	.40	-
A Iron	3.57	2.31	.70	.025	.032	.03	.06	.03	.01	.12	.006
B Iron	3.90	2.53	.67	.032	.029	.04	.06	.03	.01	.13	.006

TABLE 2. MECHANICAL PROPERTIES

	Pearlitic	A Iron	B Iron
Modulus of Elasticity E (Tension/Compression) GPa	84/108	76/78	45/56
Yield Strength, .2% S_y MPa	185	89	73
Ultimate Strength (True Fracture Strength, σ_f) MPa	228	104	85
True Fracture Ductility (ε_f)	0.0122	0.0096	0.0086
Bulk Hardness	180 BHN (3000 kg)	80 BHN (500 kg)	74 BHN (500 kg)
Eutectic Cell size mm	0.14	0.52	0.75
ASTM A247 Flake Designation	∿60% Type A, ∿40% Type D	∿50% Type A, ∿50% Type D	∿50% Type B, ∿50% Type D
Size	4	5	2

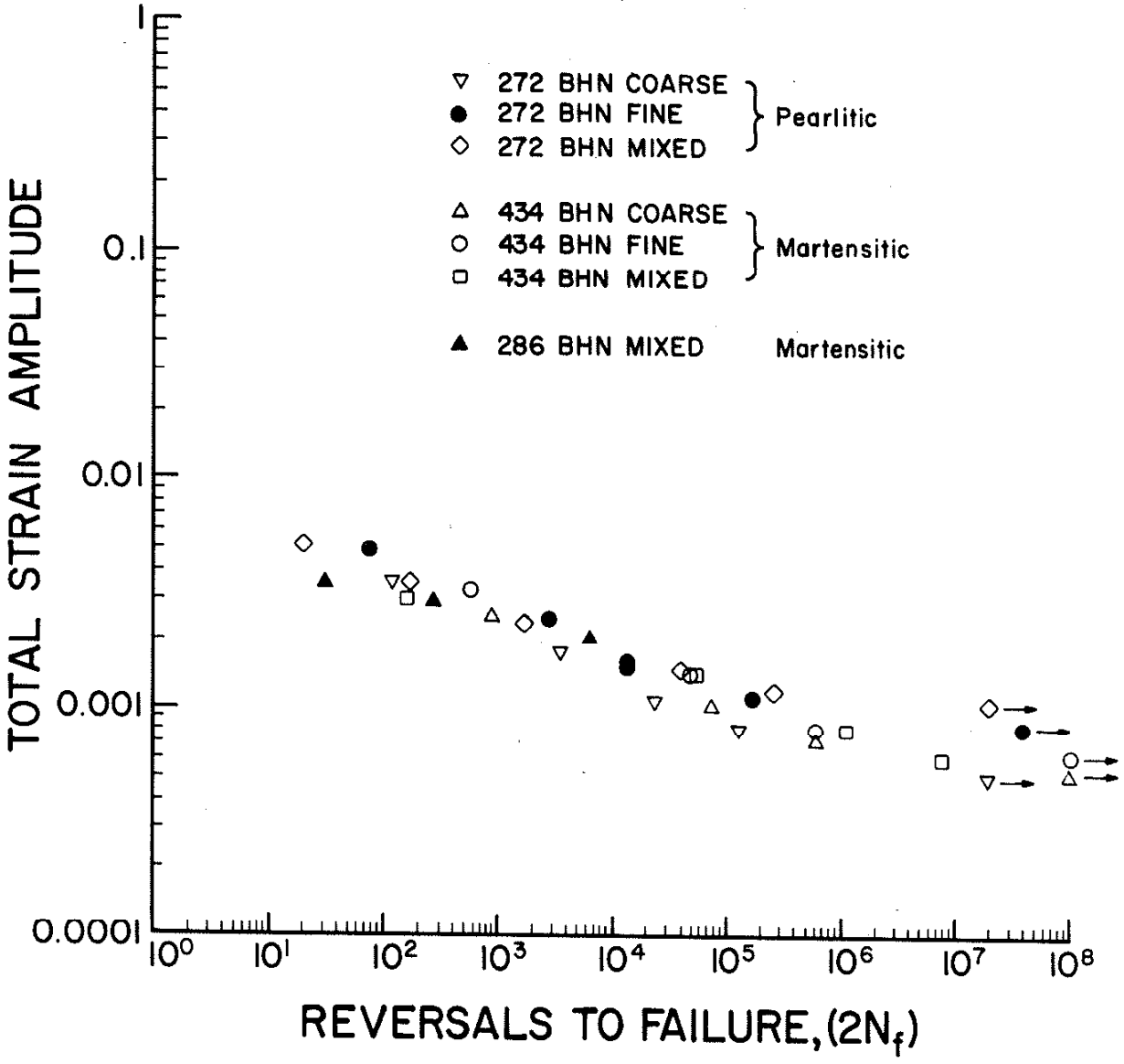

FIG. 1 EFFECT OF MATRIX MICROSTRUCTURE AND HARDNESS ON THE FATIGUE OF GRAY IRONS [10].

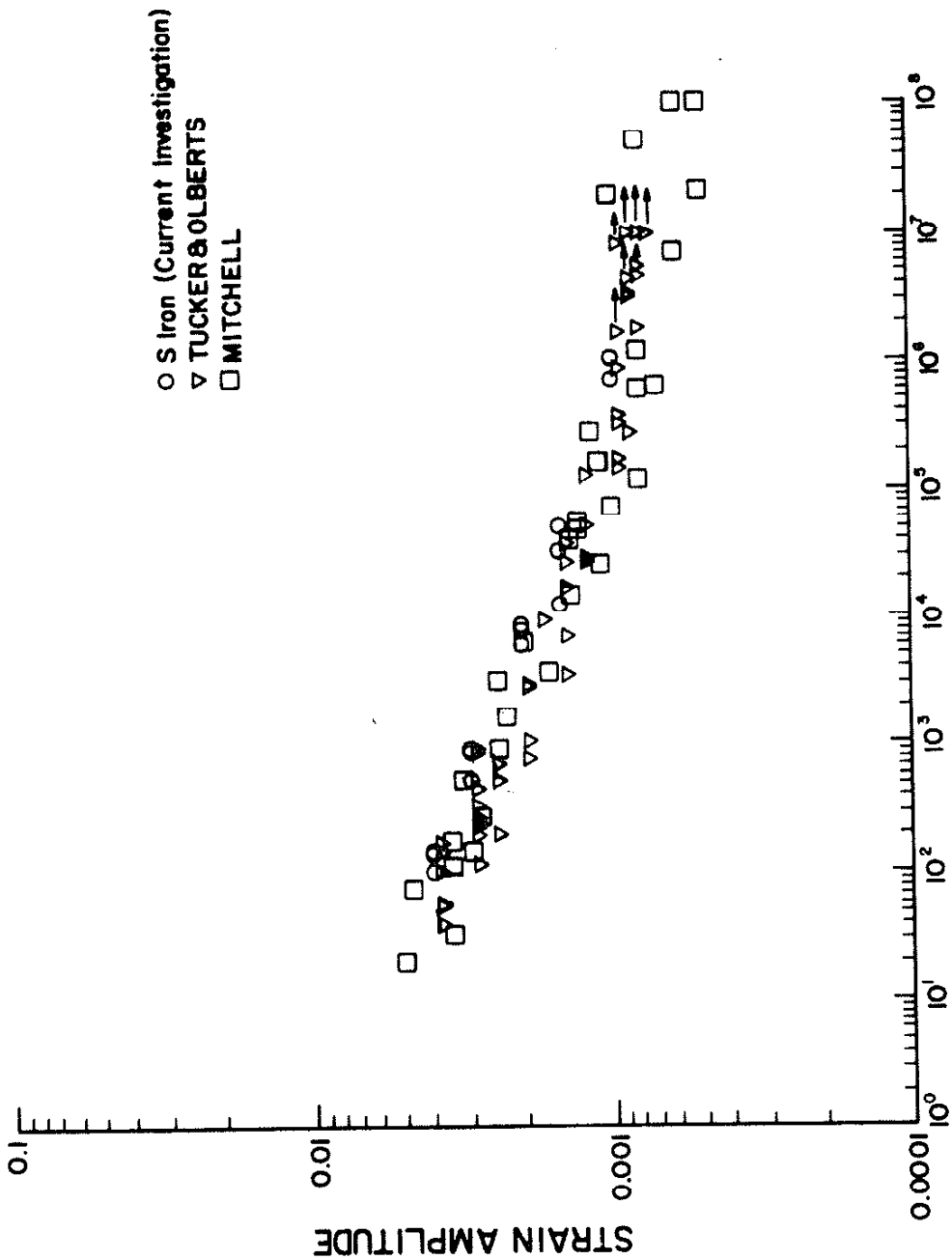

FIG. 2 STRAIN LIFE FATIGUE DATA FOR A VARIETY OF GRAY IRONS.

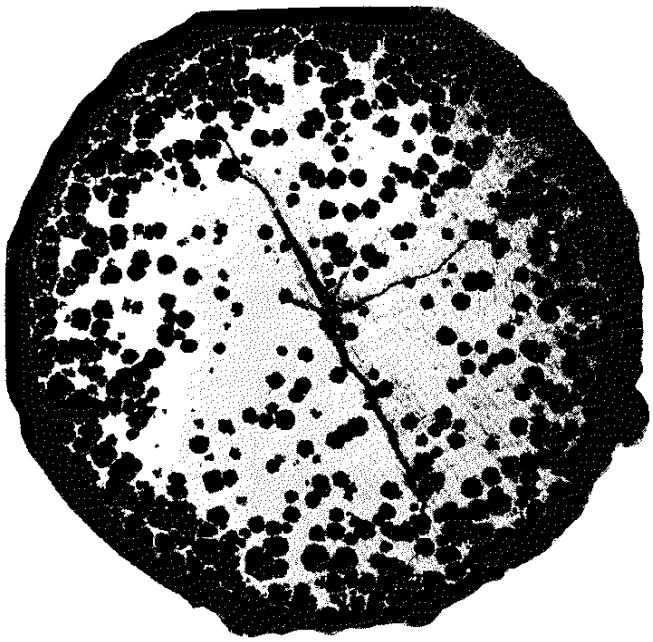

AT THE START OF SOLIDIFICATION

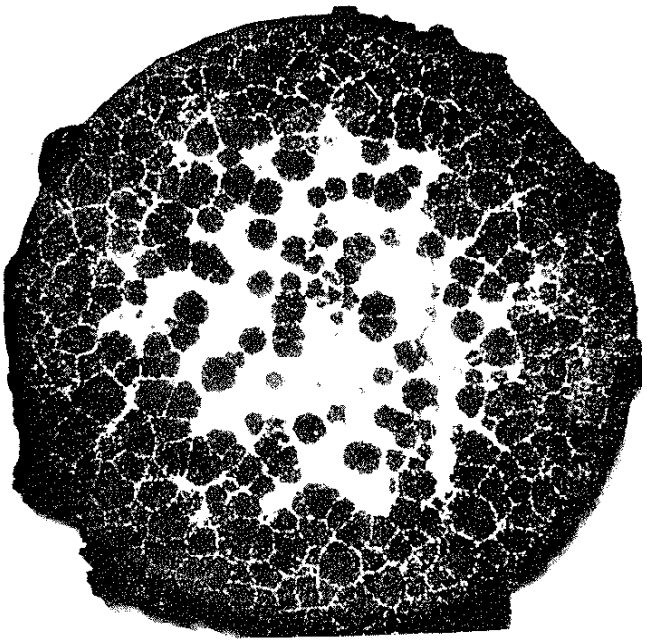

DURING SOLIDIFICATION

STRUCTURE OF BARS QUENCHED
DURING SOLIDIFICATION

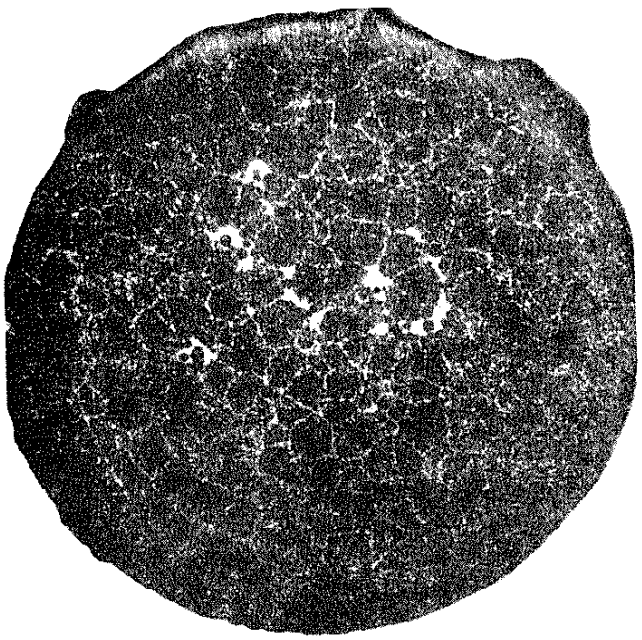

AFTER THE EUTECTIC HAD ALMOST
COMPLETELY SOLIDIFIED

FIG. 3 STRUCTURE OF CAST IRON DURING SOLIDIFICATION

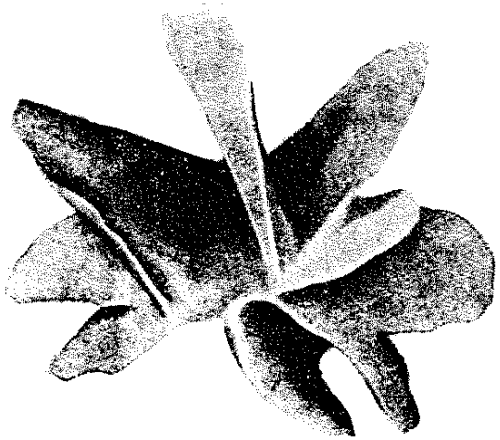

COARSE GRAPHITE

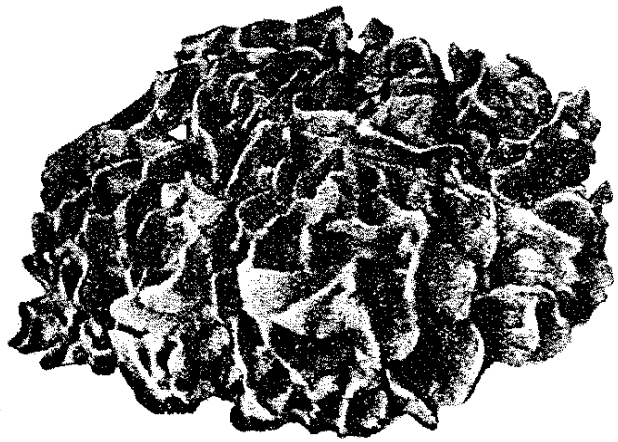

FINE GRAPHITE

MODELS OF THE THREE-DIMENSIONAL STRUCTURE OF FLAKE GRAPHITE (AFTER BUNIN, MALINOCHKA AND FEDEROVA).

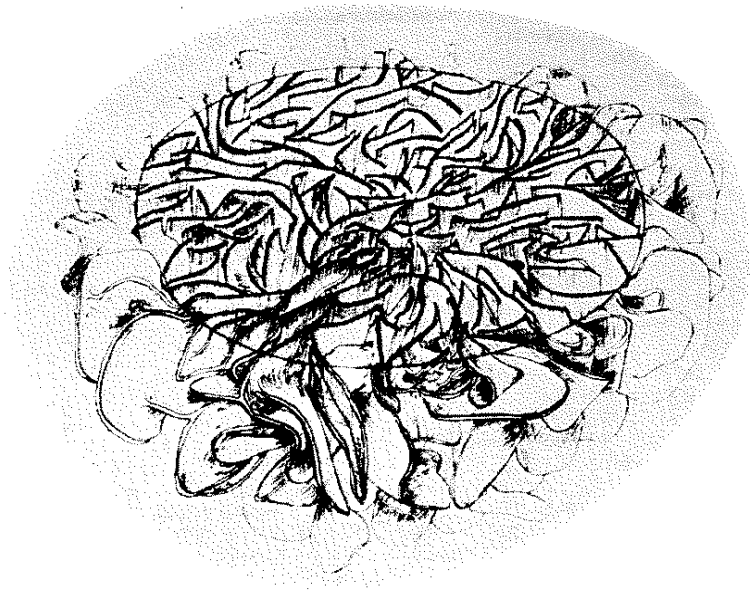

THREE-DIMENSIONAL GRAPHITE STRUCTURE AFTER DEEP ETCHING

FIG. 4 GRAPHITE STRUCTURE WITHIN EUTECTIC CELL

PEARLITIC GRAY IRON

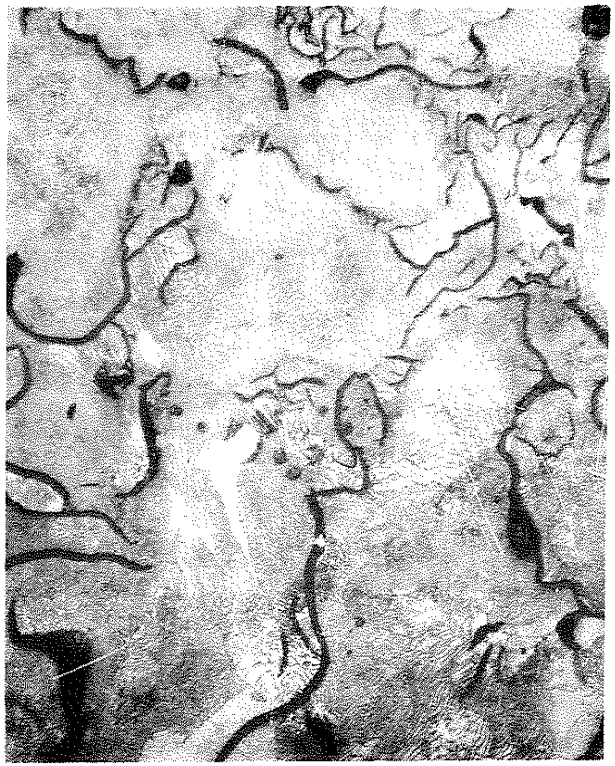

TYPE A, ~60 %
TYPE D, ~40 %
SIZE 4

2 % NITAL

FIG. 5 FLAKE FORM AND MATRIX MICROSTRUCTURE OF PEARLITIC GRAY IRON.

FERRITIC GRAY IRONS

A IRON

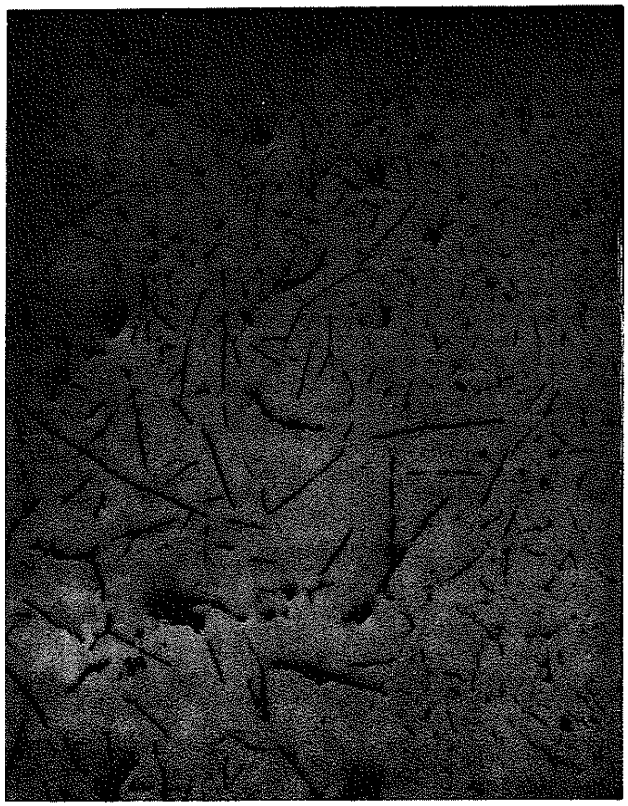

TYPE A, ~50 %
TYPE D, ~50 %
SIZE 5

B IRON

TYPE B, ~50 %
TYPE D, ~50 %
SIZE 2

FIG. 6 FLAKE FORM OF FERRITIC GRAY IRONS A AND B.

A IRON

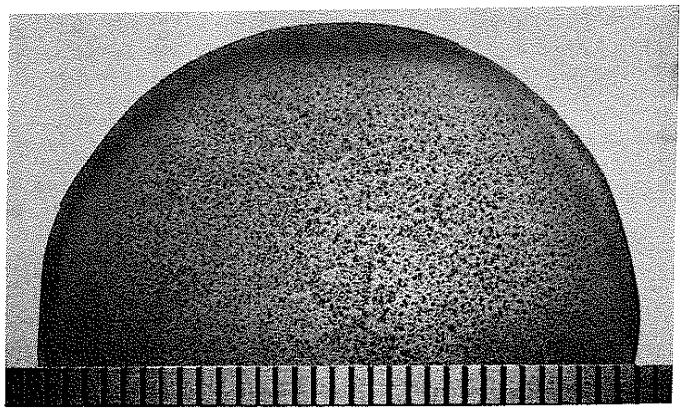

B IRON

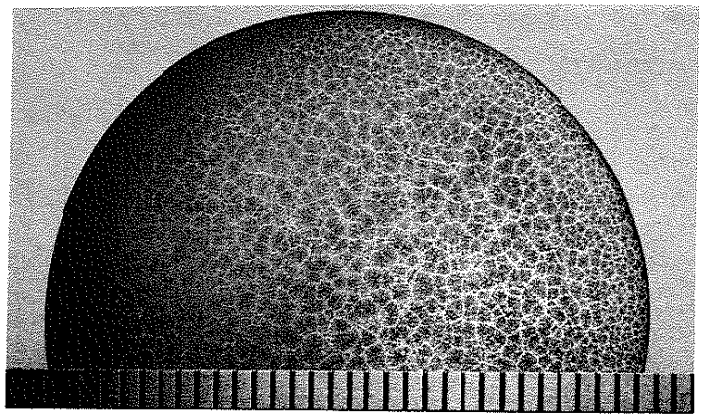

FIG. 7 EUTECTIC CELL STRUCTURE OF FERRITIC GRAY IRONS.

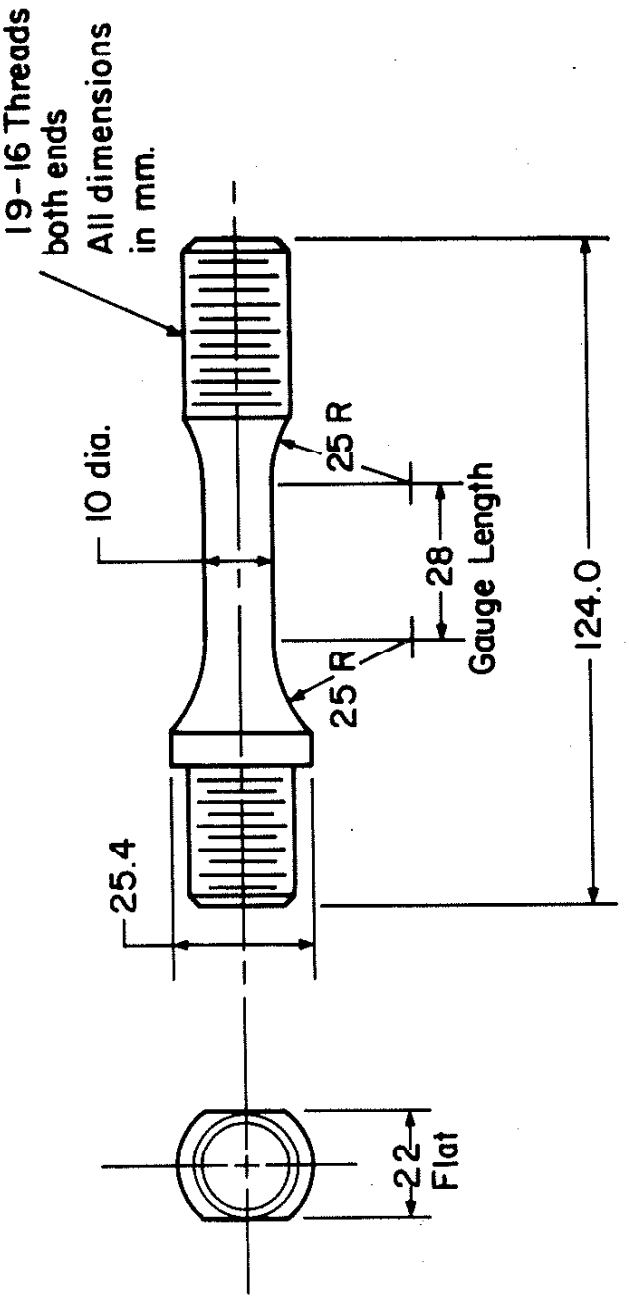

FIG. 8 TEST SPECIMEN

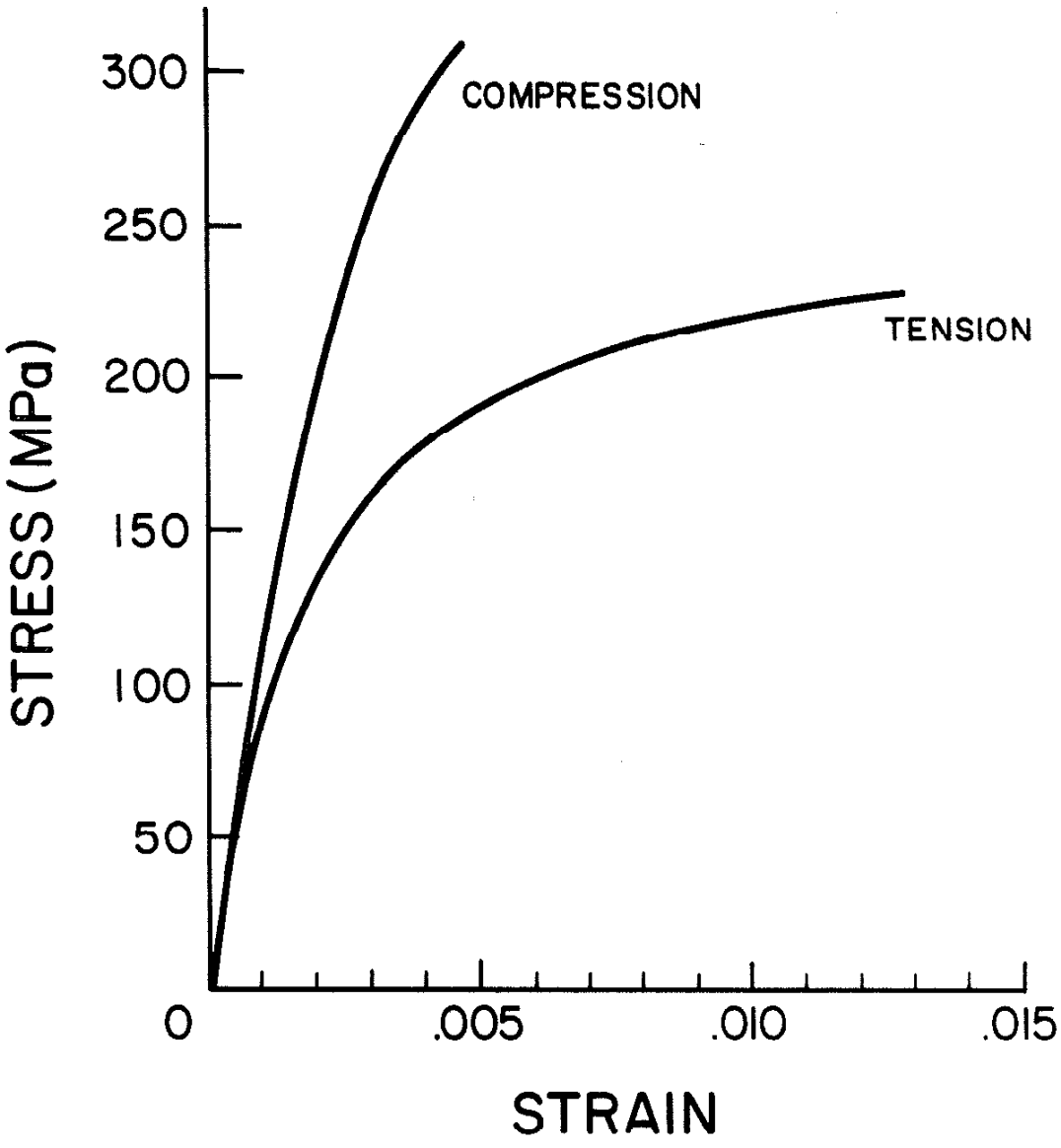

FIG. 9 MONOTONIC STRESS-STRAIN RESPONSE OF PEARLITIC GRAY IRON.

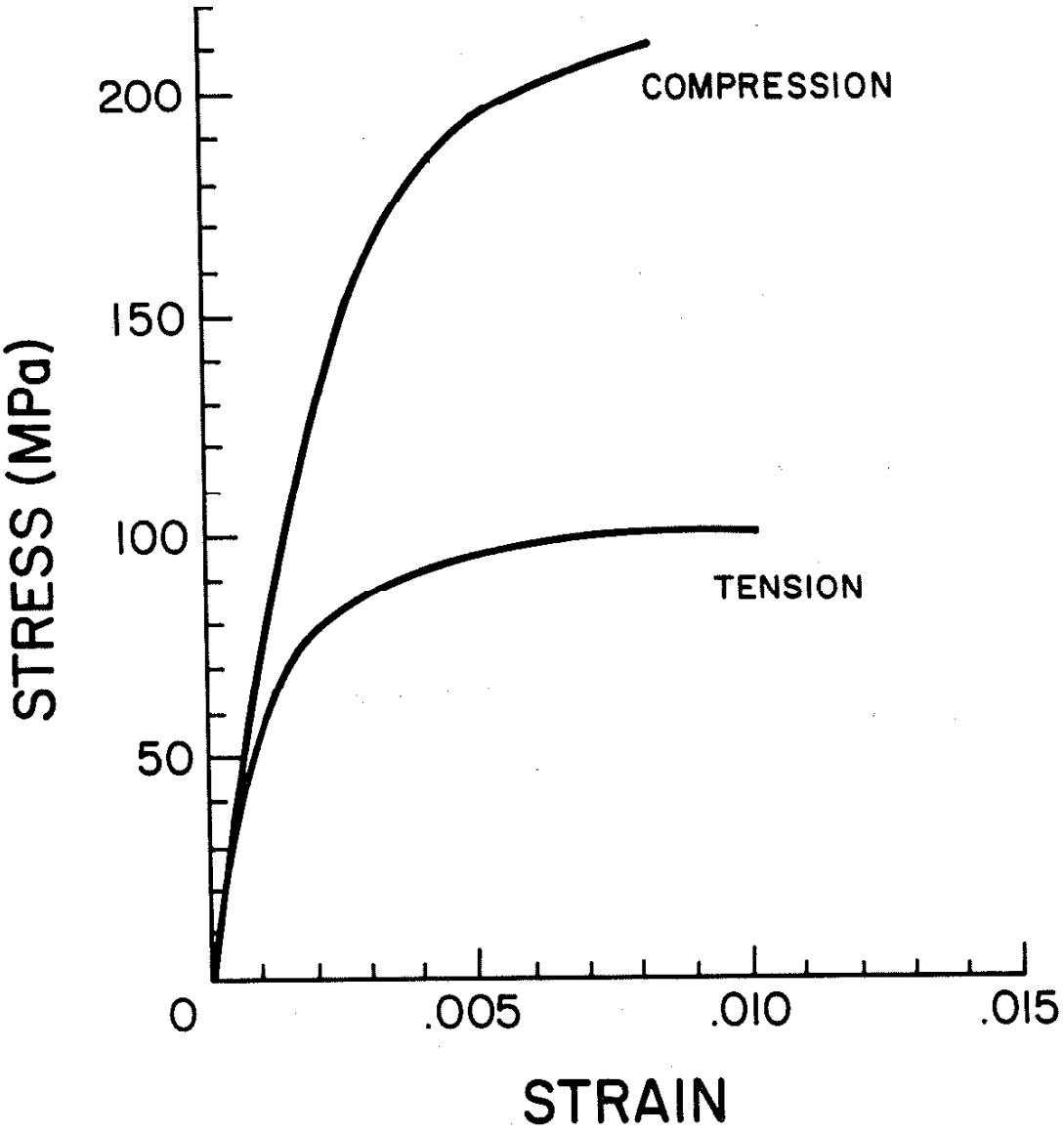

FIG. 10 MONOTONIC STRESS-STRAIN RESPONSE OF FERRITIC A IRON.

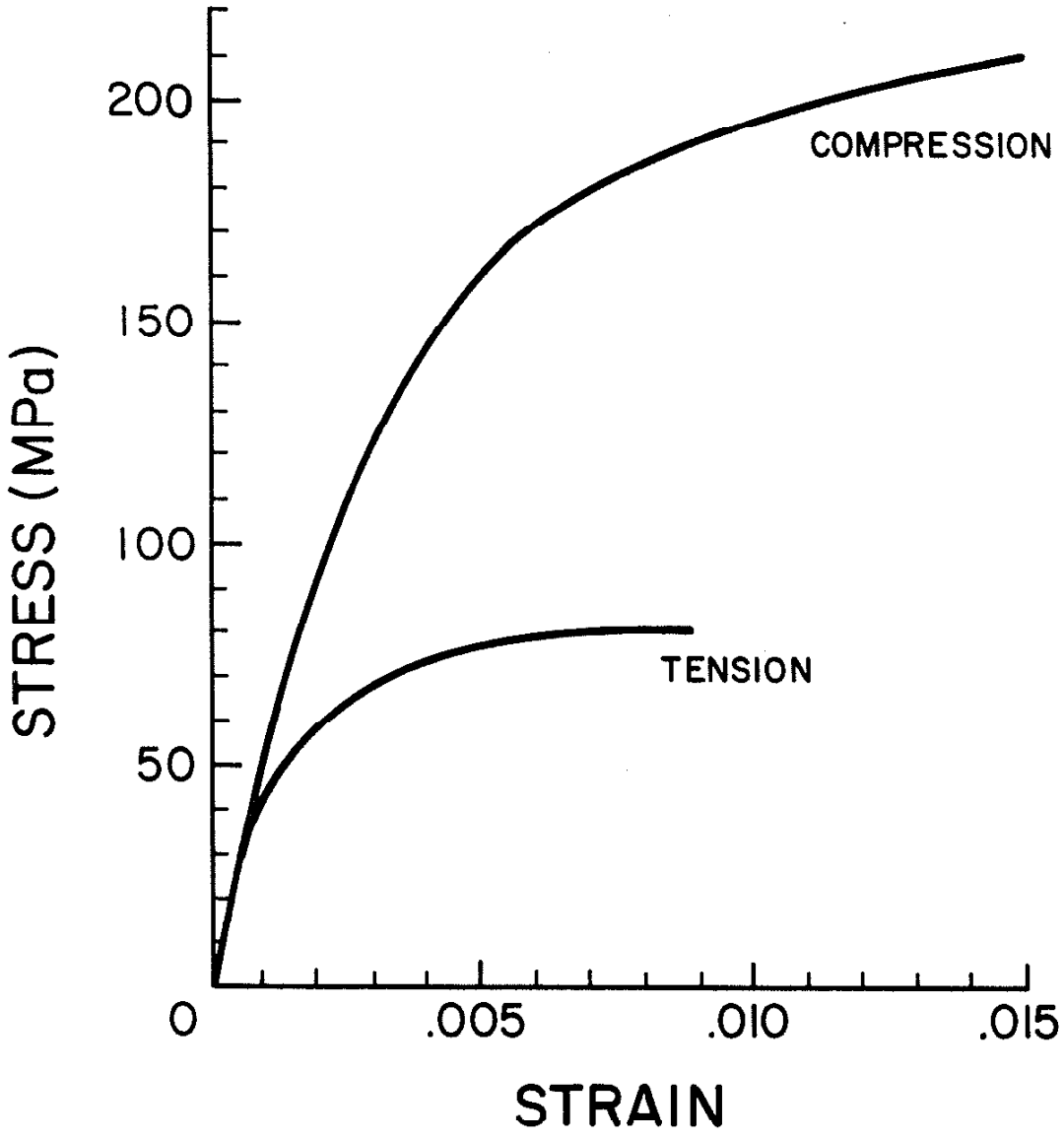

FIG. 11 MONOTONIC STRESS-STRAIN RESPONSE OF FERRITIC B IRON.

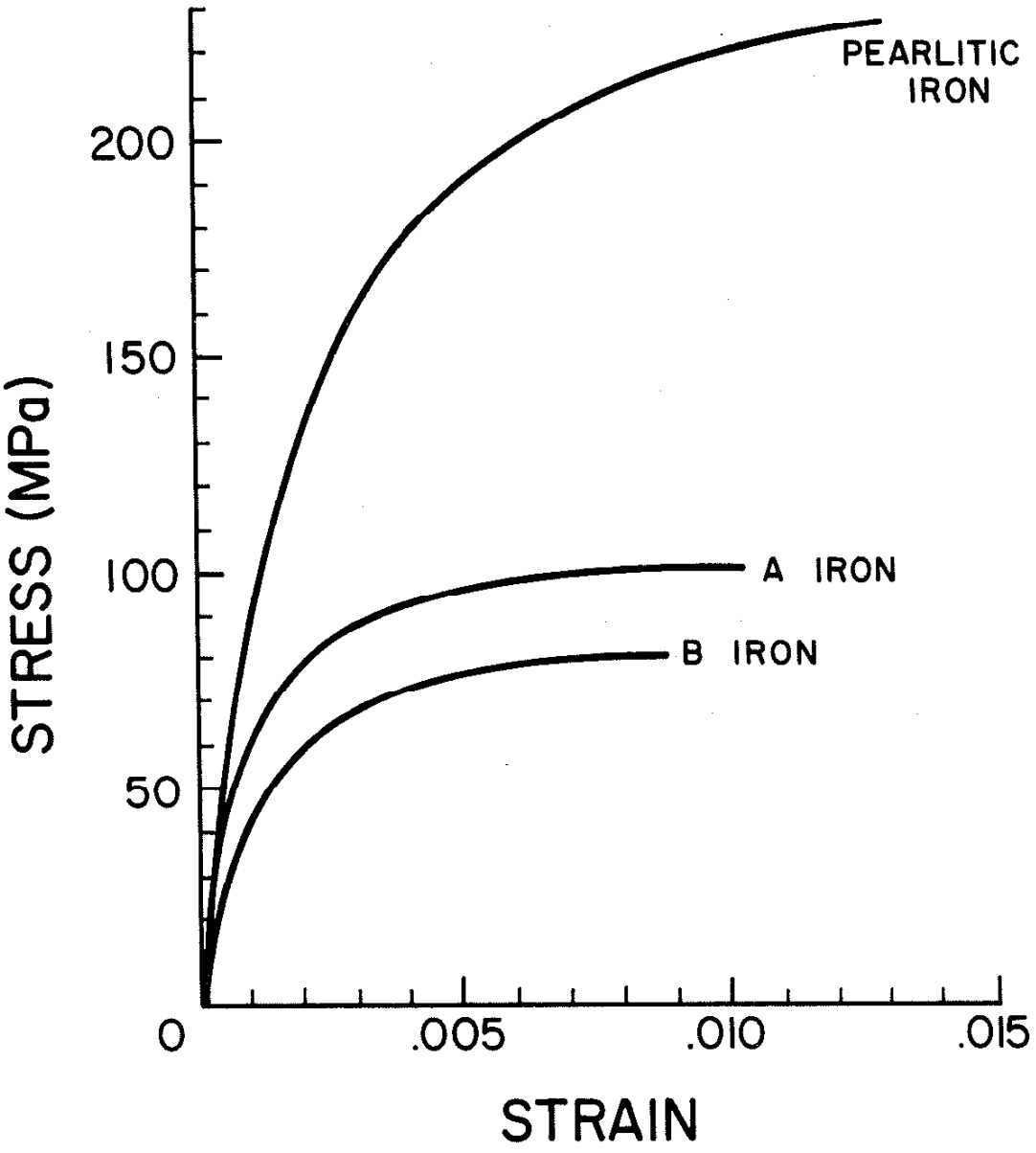

FIG. 12 MONOTONIC TENSILE STRESS-STRAIN RESPONSE OF PEARLITIC AND FERRITIC IRONS.

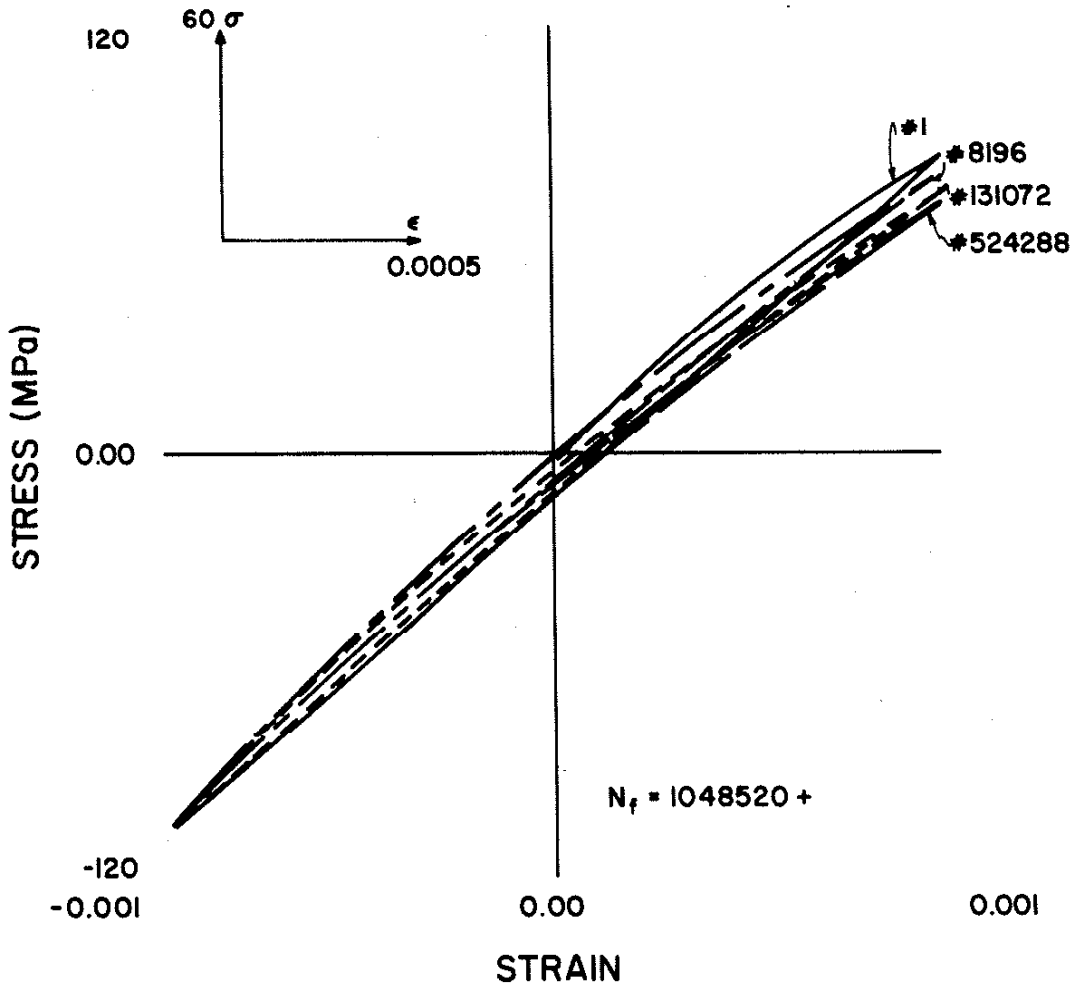

FIG. 13 HYSTERESIS RESPONSE OF PEARLITIC IRON ; $\Delta\varepsilon/2 = 0.001$.

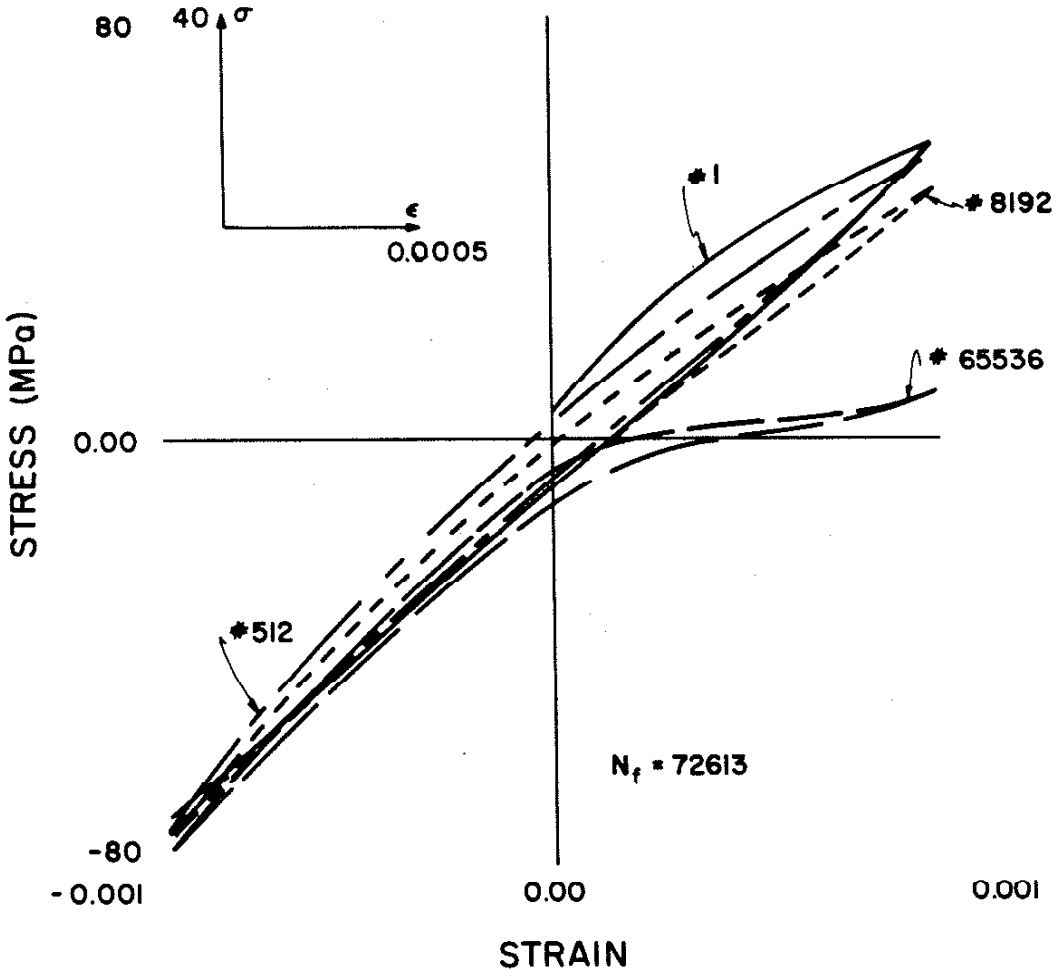

FIG. 14 HYSTERESIS RESPONSE OF A IRON ; $\Delta\epsilon/2 = 0.001$.

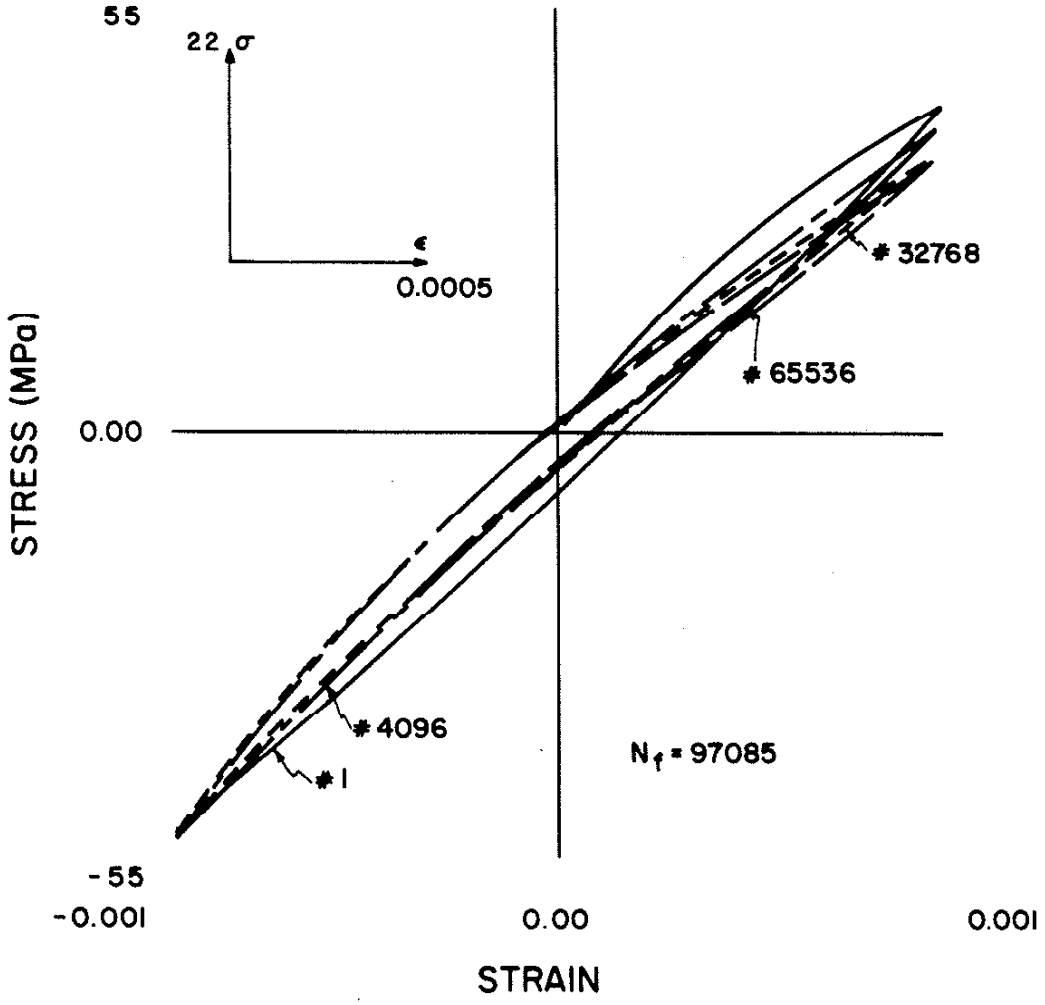

FIG. 15 HYSTERESIS RESPONSE OF B IRON; $\Delta\varepsilon/2 = 0.001$.

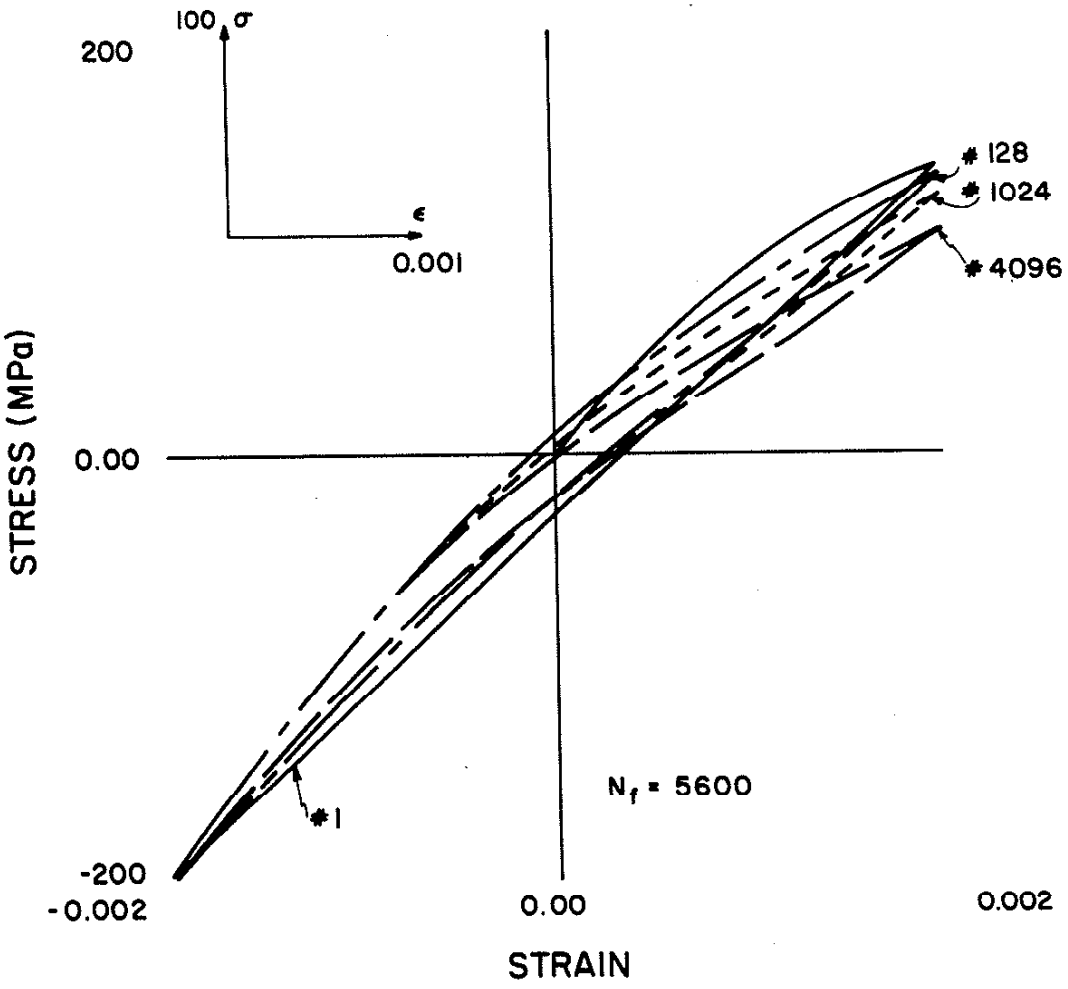

FIG. 16 HYSTERESIS RESPONSE OF PEARLITIC IRON; $\Delta\epsilon/2 = 0.002$.

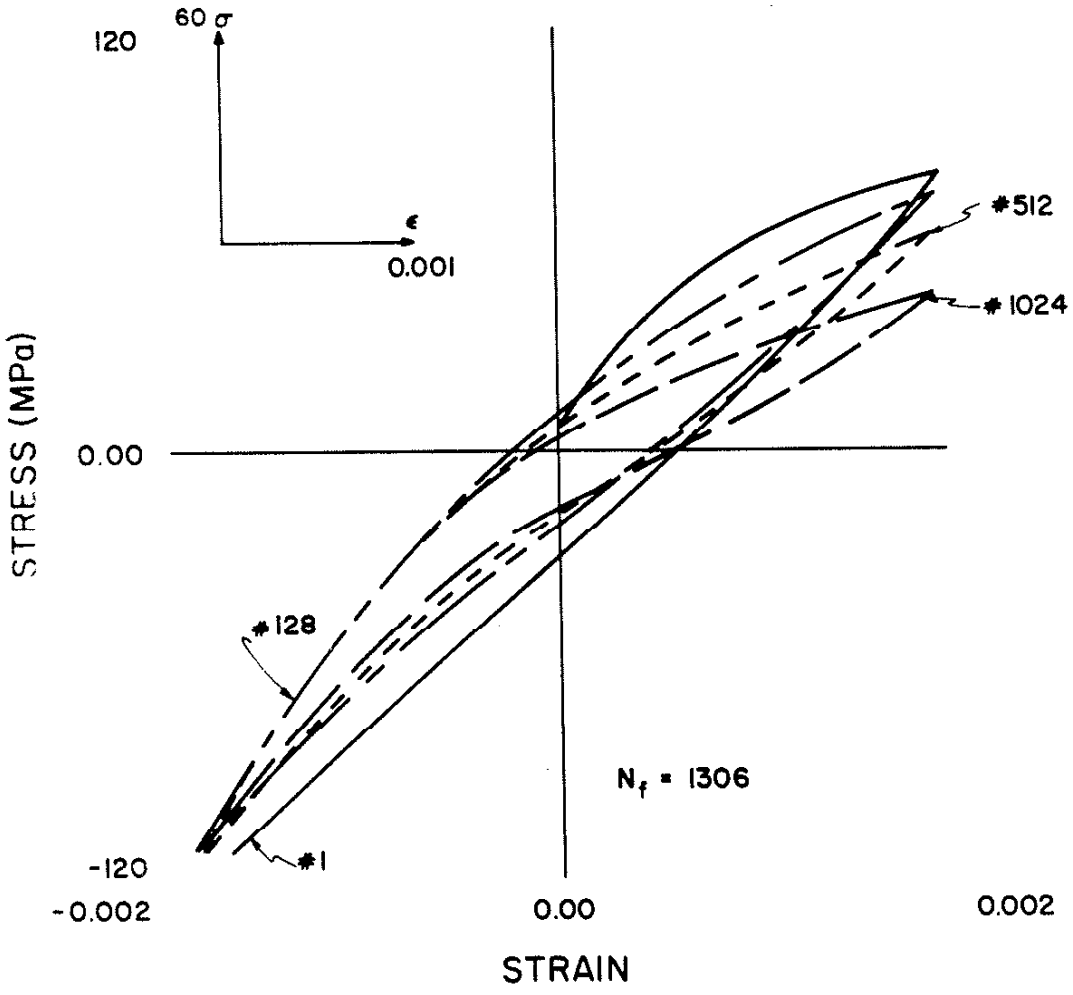

FIG. 17 HYSTERESIS RESPONSE OF A IRON; $\Delta\varepsilon/2 = 0.002$.

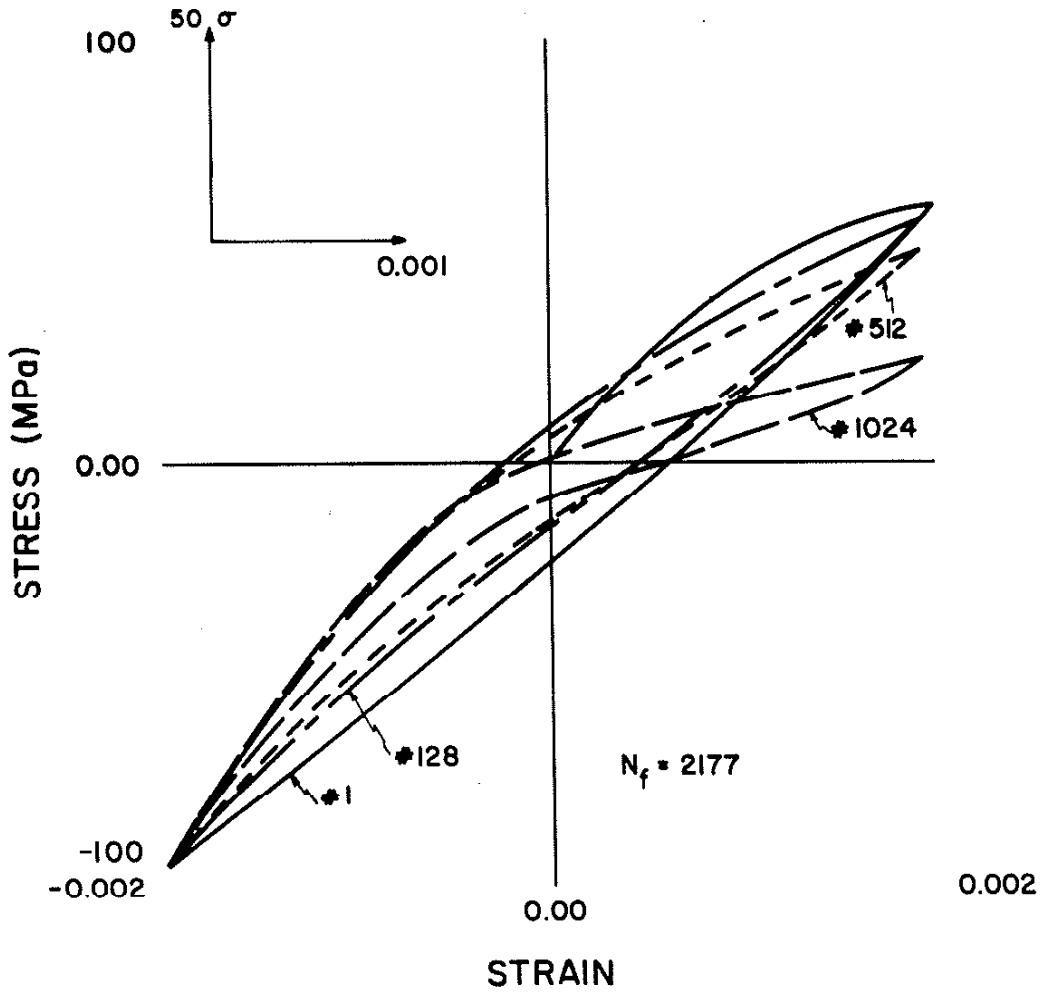

FIG. 18 HYSTERESIS RESPONSE OF B IRON; $\Delta\varepsilon/2 = 0.002$.

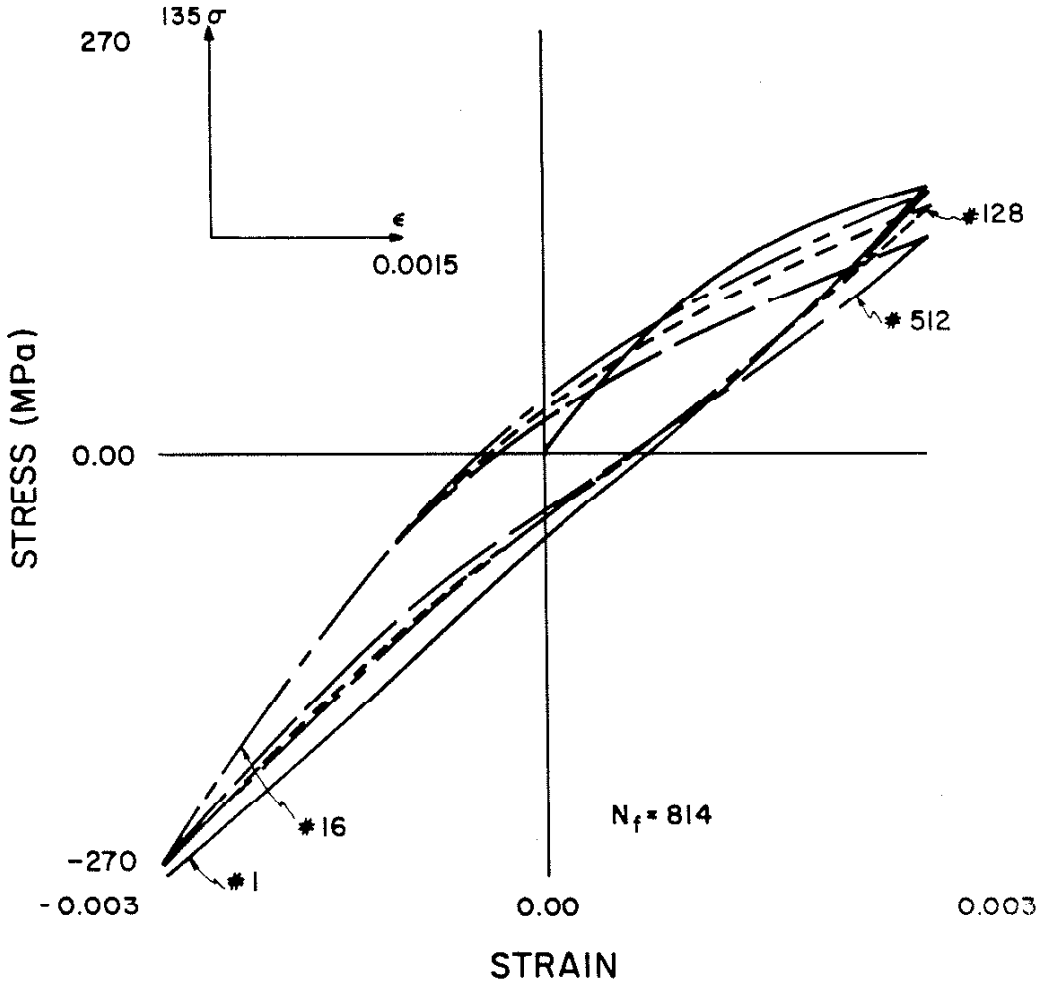

FIG. 19 HYSTERESIS RESPONSE OF PEARLITIC IRON; $\Delta\varepsilon/2 = 0.003$.

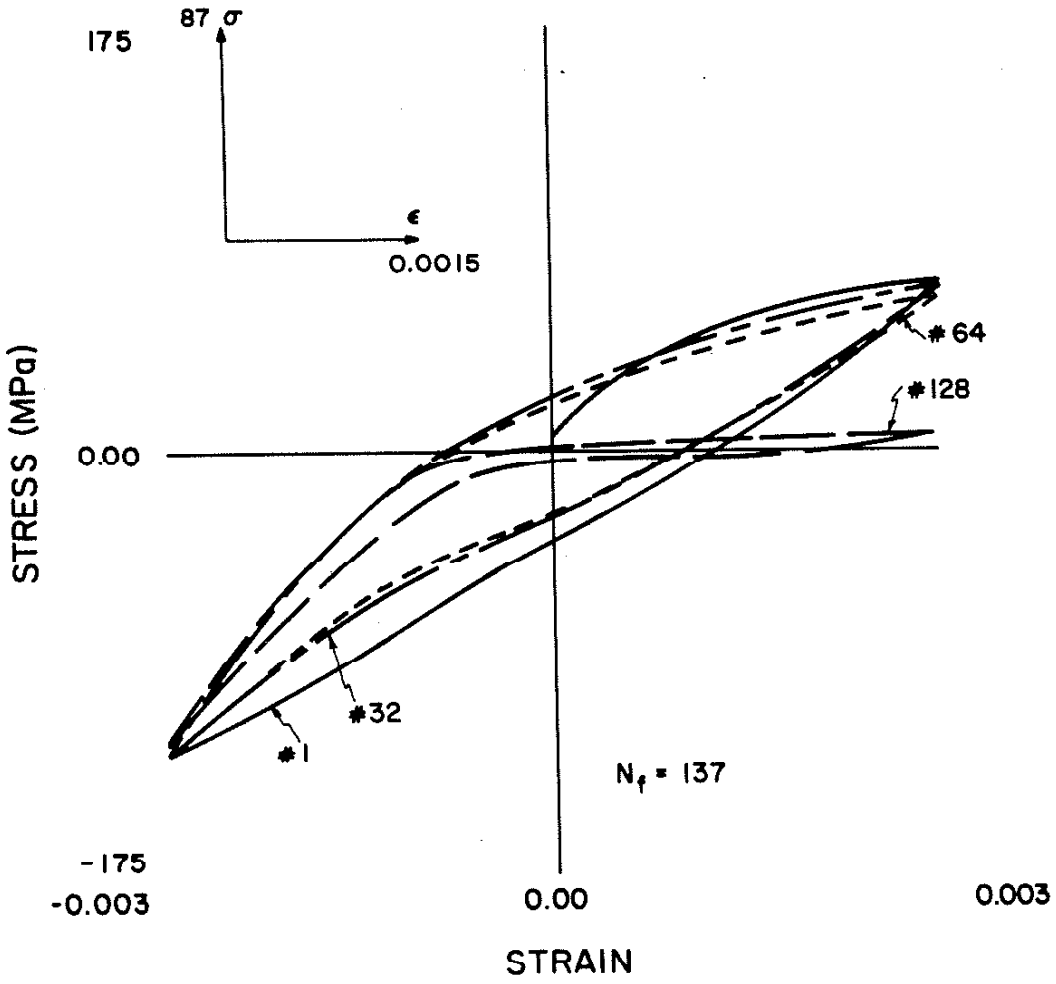

FIG. 20 HYSTERESIS RESPONSE OF A IRON; $\Delta\varepsilon/2 = 0.003$.

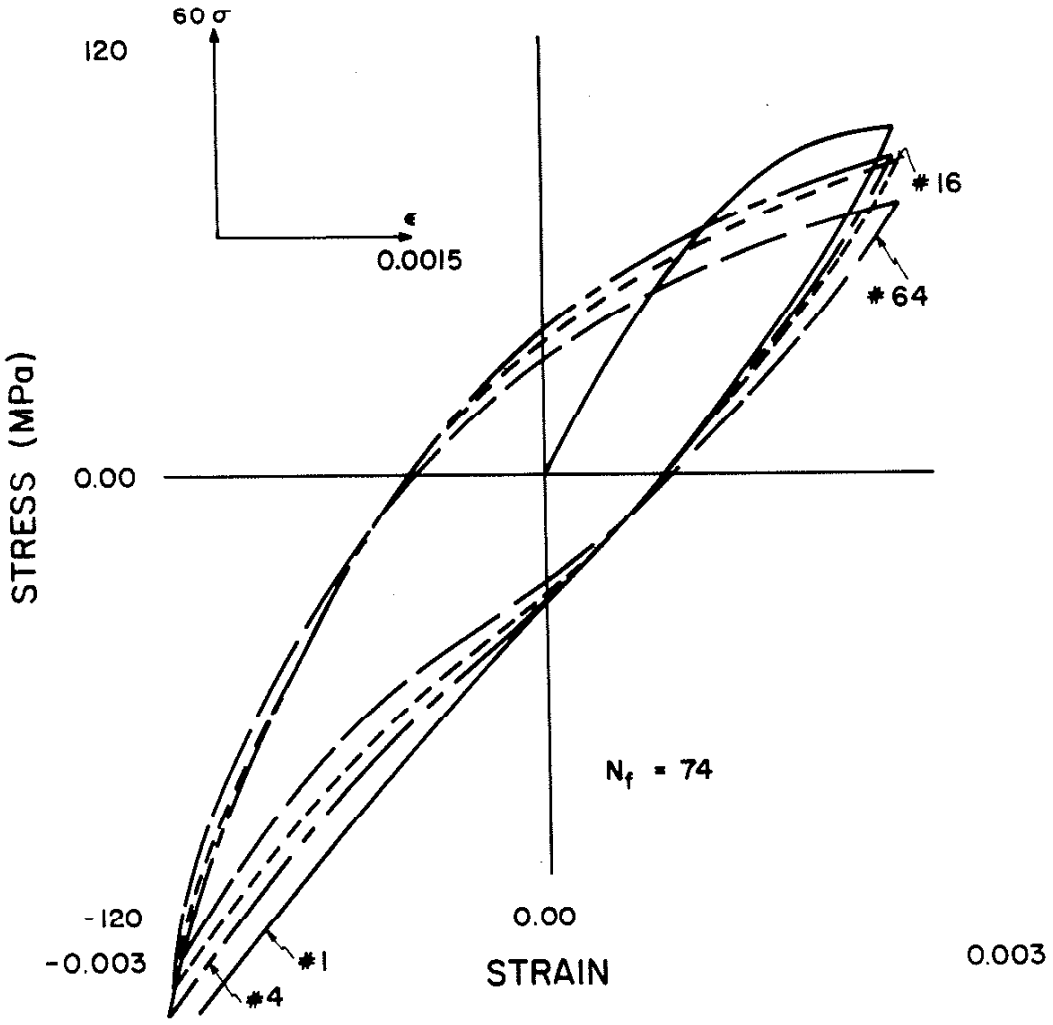

FIG. 21 HYSTERESIS RESPONSE OF B IRON; $\Delta\varepsilon/2 = 0.003$.

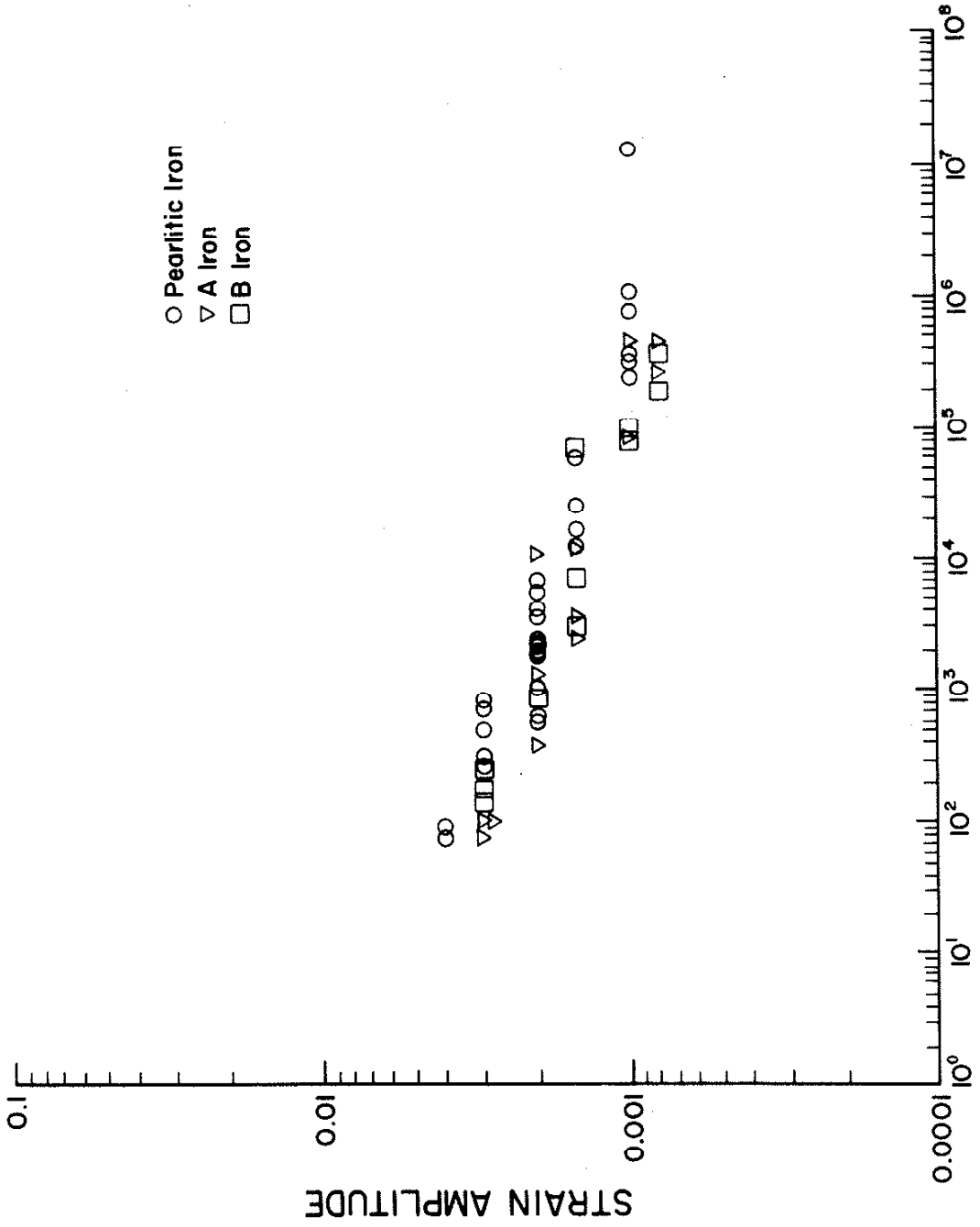

FIG. 22 STRAIN-LIFE FATIGUE DATA FOR THE THREE IRONS TESTED.

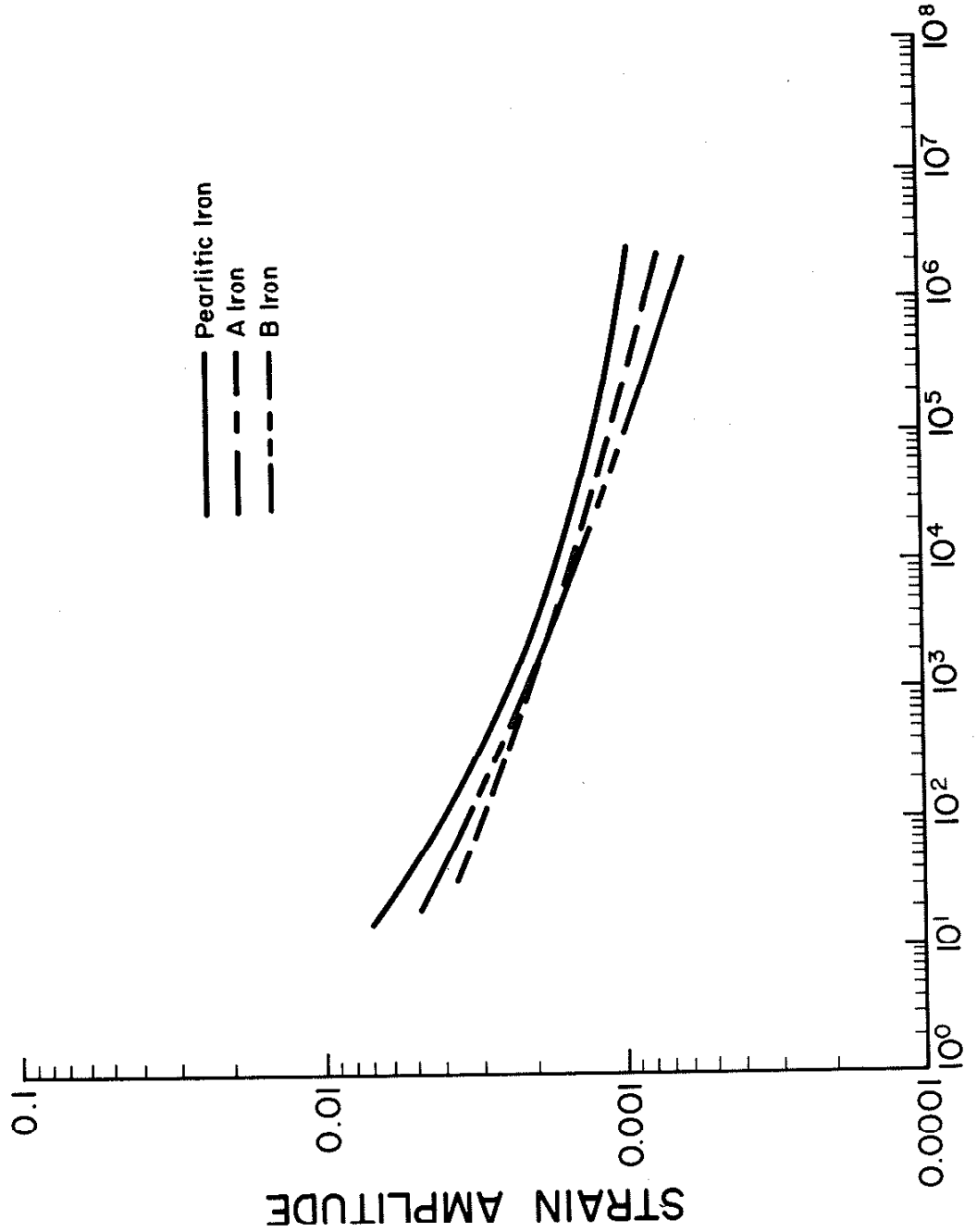

FIG. 23 STRAIN-LIFE CURVES FOR THREE IRONS TESTED.

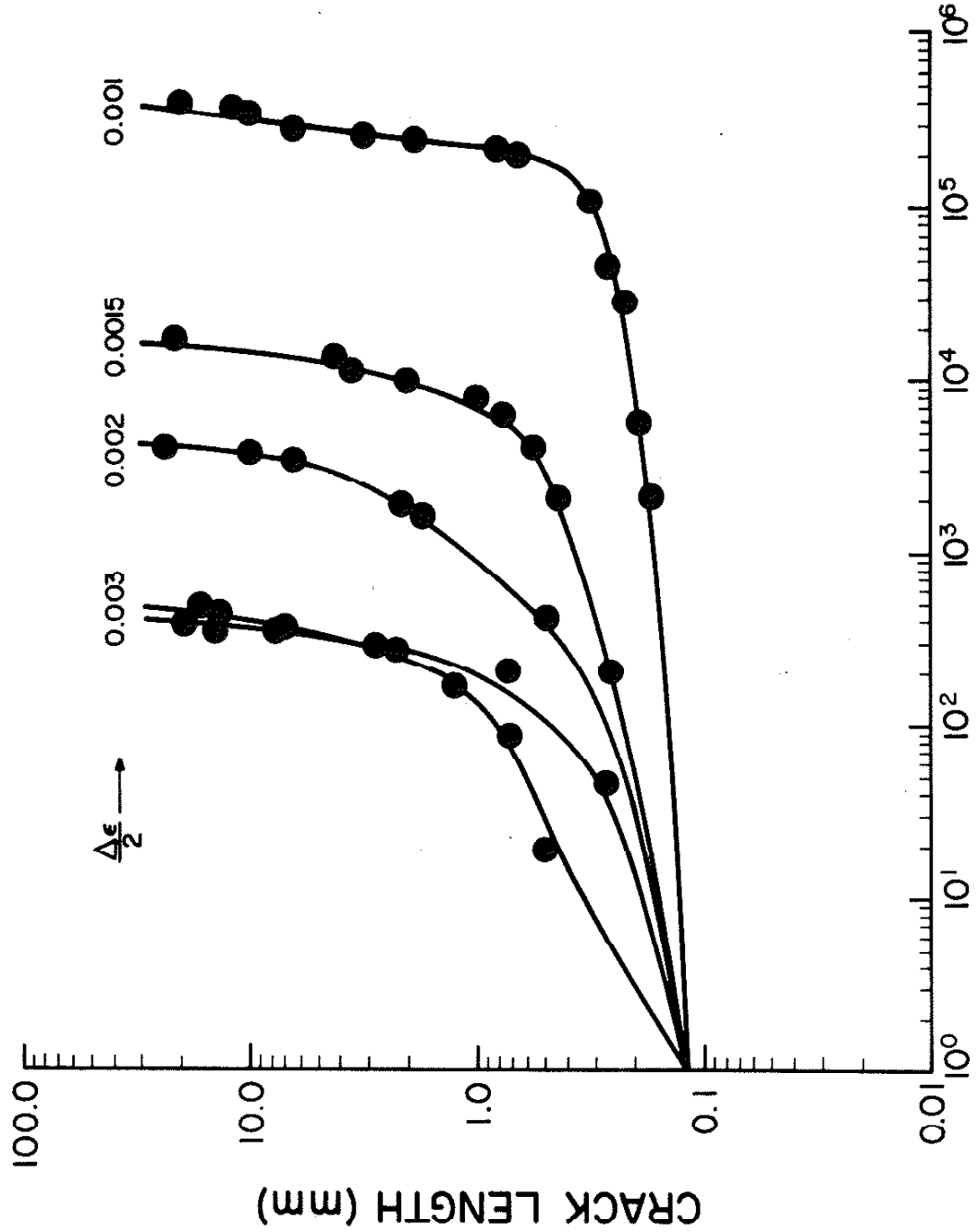

FIG. 24 CRACK LENGTH VERSUS APPLIED CYCLES MEASURED FROM SURFACE REPLICAS.

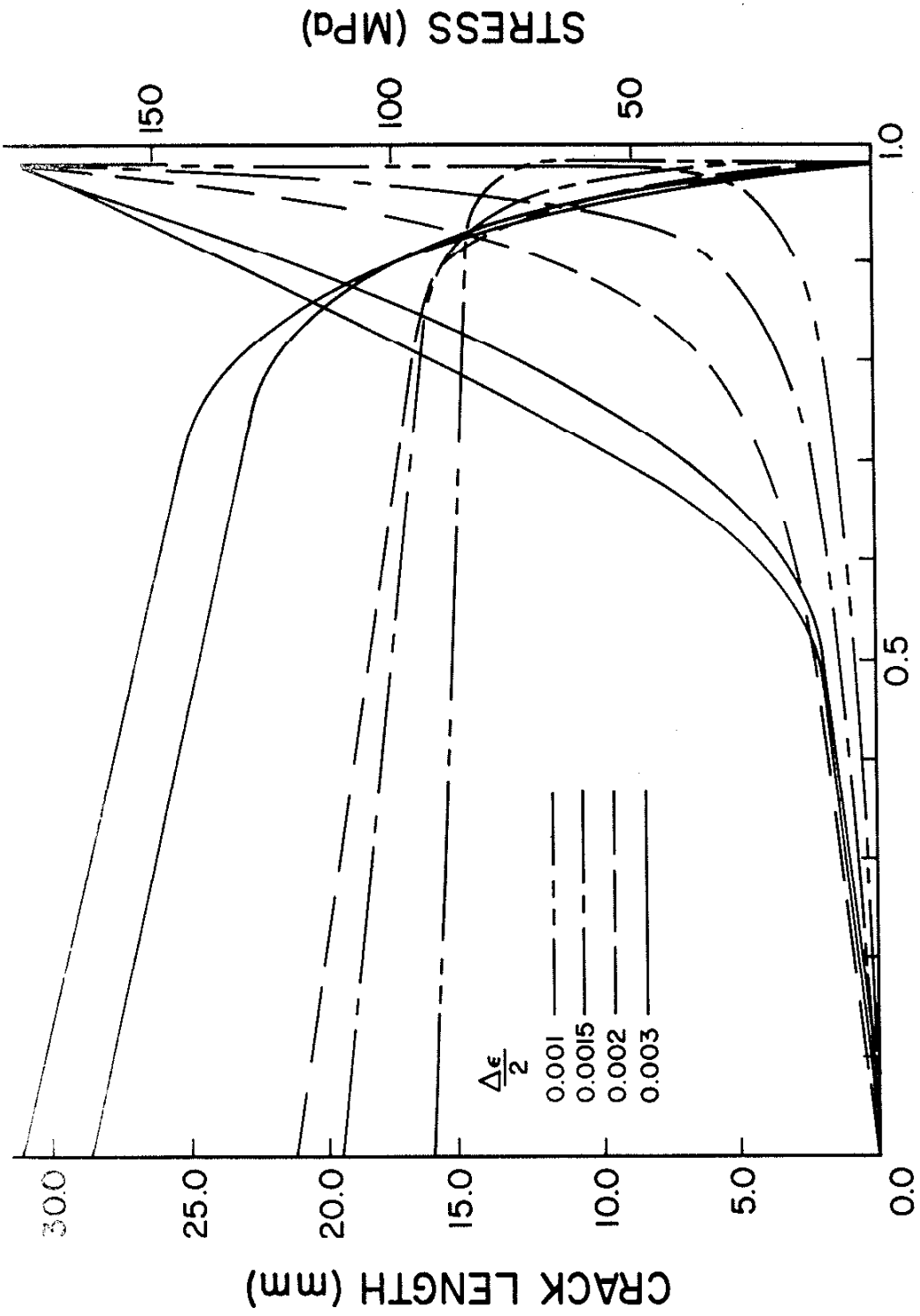

FIG. 25 CRACK GROWTH (LOWER CURVES) AND STRESS (UPPER CURVES) VERSUS APPLIED CYCLES/CYCLES TO FAILURE FOR PEARLITIC GRAY IRON.

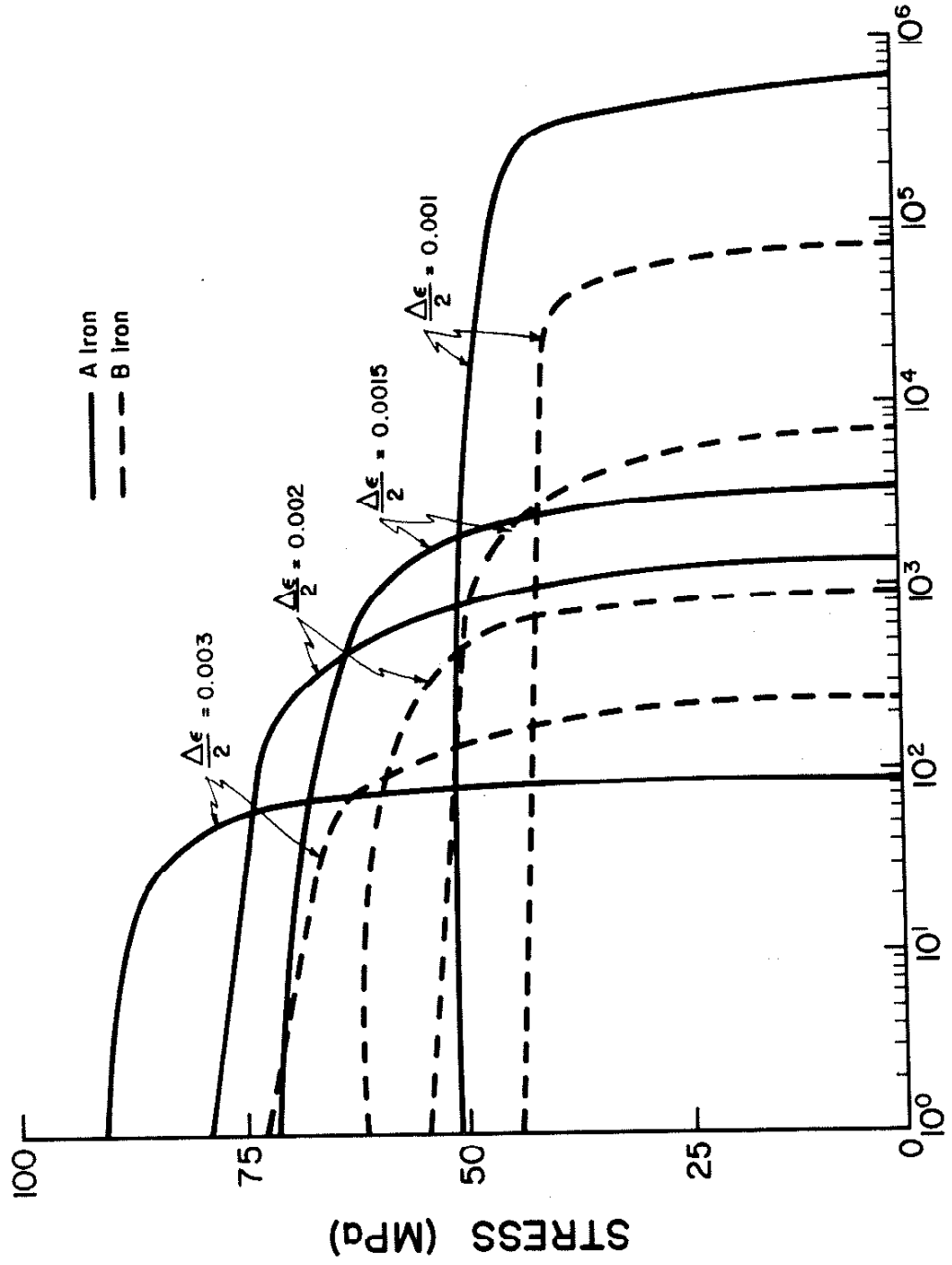

FIG. 26 LOAD DROP VERSUS APPLIED CYCLES FOR FERRITIC IRONS.

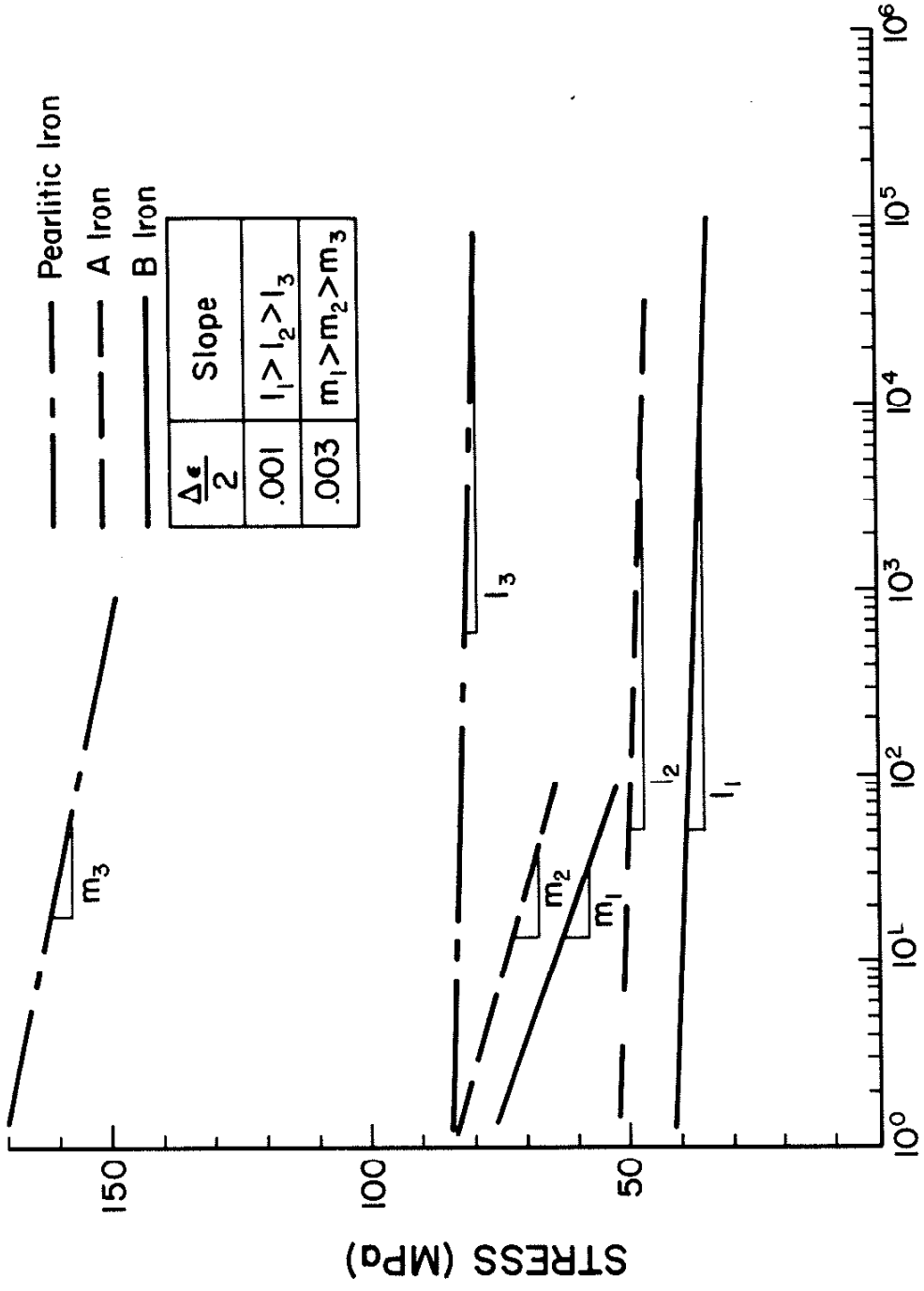

FIG. 27 SCHEMATIC REPRESENTATION OF LOAD DROP VERSUS APPLIED CYCLES OF THE THREE TEST IRONS.

APPENDIX A

FATIGUE DATA

Pearlitic Iron

Specimen	$\frac{\Delta G}{2}$	N_{10}	N_f
102	.003	---	500
103	.002	---	6,500
105	.003	400	700
108	.002	---	4,000
109	.0015	7,190	16,180
112	.004	40	87
114	.001	748,500	750,000
116	.004	41	74
117	.0015	7,940	12,070
119	.0015	10,230	12,000
121	.001	77,500	300,000
123	.002	1,930	3,520
125	.003	150	311
126	.0015	10,650	24,690
128	.002	900	1,740
129	.002	1,490	2,290
130	.001	220,000	233,470
131	.002	1,920	2,030
132	.002	1,590	2,360
133	.002	1,770	1,800
136	.002	1,470	1,950
Ferritic Irons			
A1	.002	---	1,361
A2	.0008	---	72.5×10^5
A3	.003	---	74
A4	.003	---	52
A5	.0095	8,461	449,758
A6	.001	155	1,306
A9	.002	174	1,306

Ferritic Irons (Continued)

Specimen	$\frac{\Delta G}{2}$	N_{10}	N_f
A10	.0028	65	74
A11	.0015	284	11,062
A12	.0015	335	2,408
A13	.001	1,025	10,528
A14	.002	171	1,369
A15	.0008	52	471,827
A16	.0015	257	3,414
B2	.002	---	3,614
B3	.0015	---	69,089
B4	.003	---	257
B5	.001	638	97,085
B6	.001	487	78,800
B7	.0015	554	7,123
B8	.003	69	137
B9	.002	285	2,177
B10	.0015	501	3,075
B11	.001	1,032	94,826
B12	.00077	44	370,438
B13	.002	227	907
B14	.003	78	173
B15	.008	55	184,852
B16	.00075	---	524,288

APPENDIX B

A replicating procedure was developed to observe and monitor crack formation and growth. Initiation and development of crack systems including the failure crack, which does not dominate until late in the specimen life, are permanently recorded with this technique which allows the entire specimen surface to be recorded at specific periods during the specimen life. Quantitative crack growth can be determined by observing a particular crack system in a sequence of replicas taken throughout a fatigue test. Qualitative observations of the amount and extent of crack development can be made at any period in the specimen life.

A. Technique

To obtain clear resolution of the graphite structure in gray iron, the specimen surface must be finely polished to eliminate machining or rough polishing marks from obscuring fine details of crack development. Specimens were mounted in a lathe and rotated while a pneumatic rotary polishing rod, wrapped with emory paper and felt, was used to mechanically polish the gauge section. Rough polishing was done with the emery paper with final polishing being accomplished by saturating the felt with 0.3 micron alumina metallographic powder mixed in water, similar to techniques used in metallography laboratories.

Once an acceptable polish was obtained, a fatigue test to monitor crack formation and growth could be started. It was desired to obtain between 10 and 15 surface replicas throughout the test. From base line fatigue data approximate lives were known and replicas were taken at about every 8% of the expected life. Peak tensile load was monitored and if a

decrease of about 4% was observed before the expected 8% increment in life, a replica was taken to detect the cause of the load drop.

Equipment used to obtain the replicas include: 0.034 mm thick acetyl cellulose replicating film, acetone, methyl alcohol, hypodermic syringe, polishing cloth, glass slides, and tweezers. To obtain a surface replica the specimen surface must be clean and easily accessible. A procedure for removal and remounting of the strain extensometer during the test is outlined at the end of this appendix. A nonfibrous polishing cloth with methyl alcohol was used to clean the specimen of fingerprints and remnants left from previous replicas. To insure that the total surface is recorded, the specimen was marked into three regions. Replicas of each of these regions were taken by holding a strip of replicating tape, cut to the width of the gauge section, loosely around the specimen. Acetone was injected between the specimen and the tape using the hyperdermic. Acetone softens the tape which is then pulled snugly against the specimen to conform to the surface topography. Approximately two minutes are required for the acetone to evaporate and the replica to harden. The replica is then easily removed from the specimen and placed between appropriately marked glass slides.

B. Observation

Many techniques can be used to observe replicas obtained as described above. Replicas can be used as photo negatives and incorporated with a photographic enlarger to make prints of the replicas. This involves the use of darkroom facilities and photographic techniques which can be expensive and time consuming, but good results can be obtained this way.

Scanning electron microscopy was also investigated as a means of observing replicas. For this technique the replica must be mounted on a

conducting surface compatible with the stage of the specific SEM being used and a conducting surface film must be placed on the tape. Sputtering of gold films and evaporation techniques were both attempted. Very good resolution of detail within the replicas were obtained with this method, but the time required for specimen preparation and the limited viewing area of the SEM made this technique unfavorable for this investigation.

Observations of the replicas were accomplished using an optical microscope. Replicas were placed between glass slides when taken, and it was not necessary to do any further preparation or remove the replica from the slides. Illumination through the replica, rather than reflecting light off the specimen gave best results.

Large crack systems which occurred near failure were photographed from replicas using a polaroid camera attachment. By tracing from the replicas near failure backwards to the replicas taken early in the life, the development of the failure crack was monitored. Examples of reduced replicas are shown in Figs. B1-B3. Note circles found in the photos of replicas are from bubbles that form when the acetone evaporates.

CRACK GROWTH TEST REPLICATING PROCEDURE

A procedure for obtaining replicas of a specimen in strain control mode is outlined below. Photographs of replicas showing the propagation of fatigue cracks during three crack growth tests are shown in Figs. B1-B3.

1. Test performed in strain control mode
2. Record hysteresis loop
3. Go to zero strain on "down" side of hysteresis loop
4. Record load $P = P^*$ at strain $\varepsilon = 0$
5. In strain control, go to $P = 0$, record $\varepsilon = \varepsilon^*$
6. Hydraulics off
7. Remove extensometer
8. Select load control mode
9. Check set point
10. Hydraulics on
11. Go to replicating load
12. Take replicas
13. Return to $P = 0$
14. Remount extensometer
15. Set offset on extensometer with amplifier zero control to strain reading of ε^*
16. Hydraulics off
17. Select strain control mode
18. Check set point
19. Hydraulics on
20. At $\varepsilon = 0$ check for $P = P^*$
21. Resume test if $P = P^*$

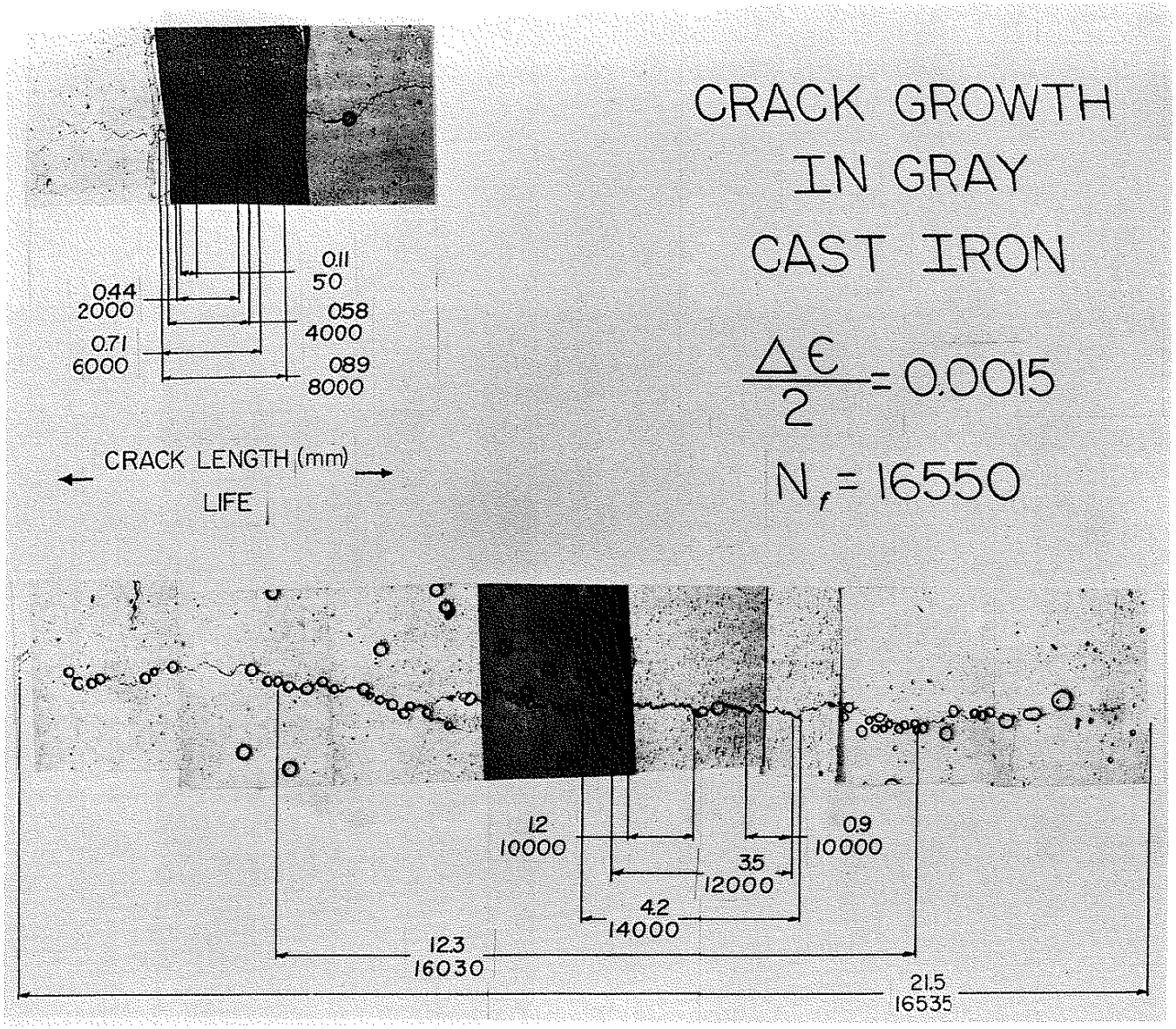

FIG. B1 CRACK DEVELOPMENT IN PEARLITIC IRON; $\Delta\varepsilon/2 = 0.0015$.

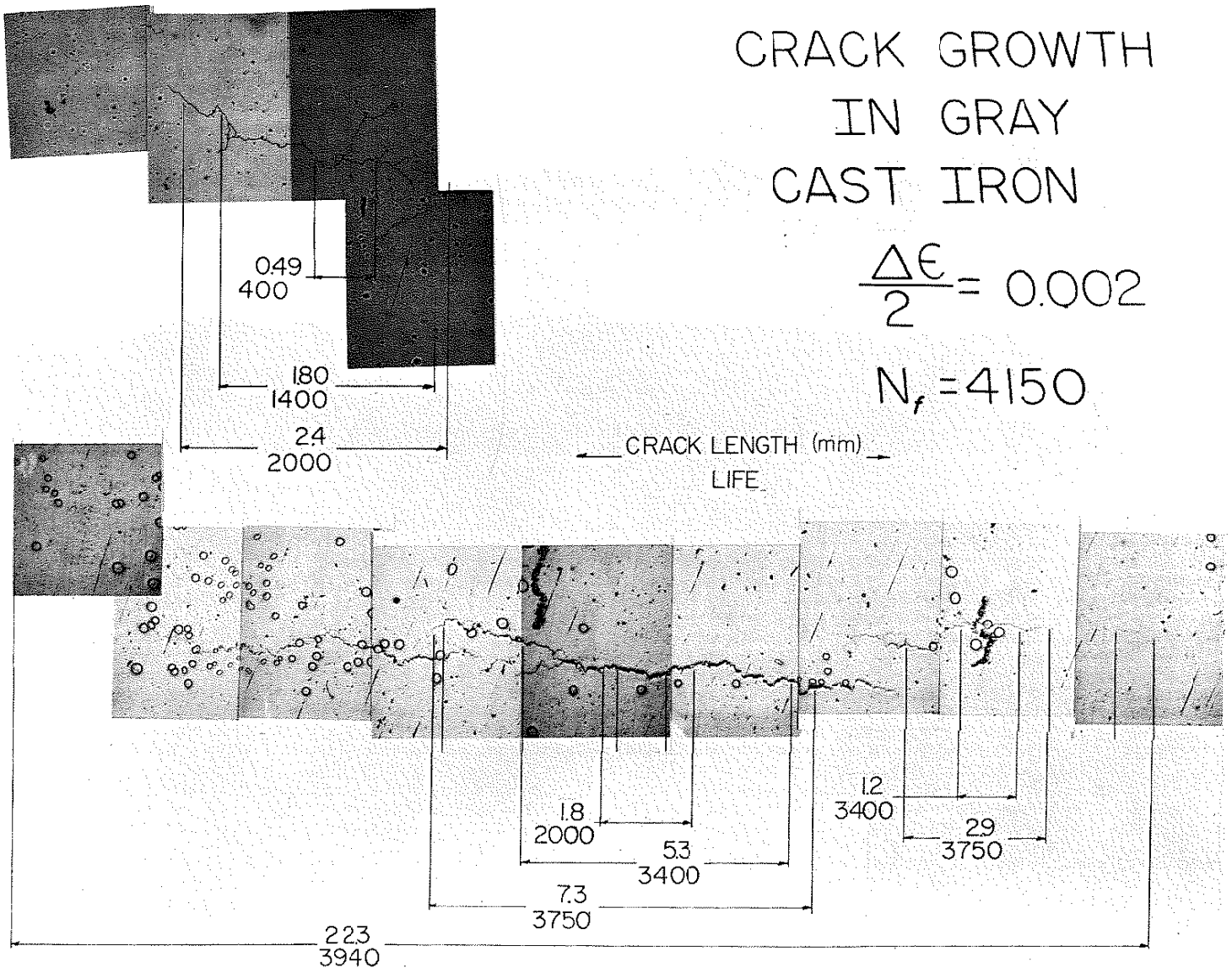

FIG. B2 CRACK DEVELOPMENT IN PEARLITIC IRON; $\Delta\varepsilon/2 = 0.002$.

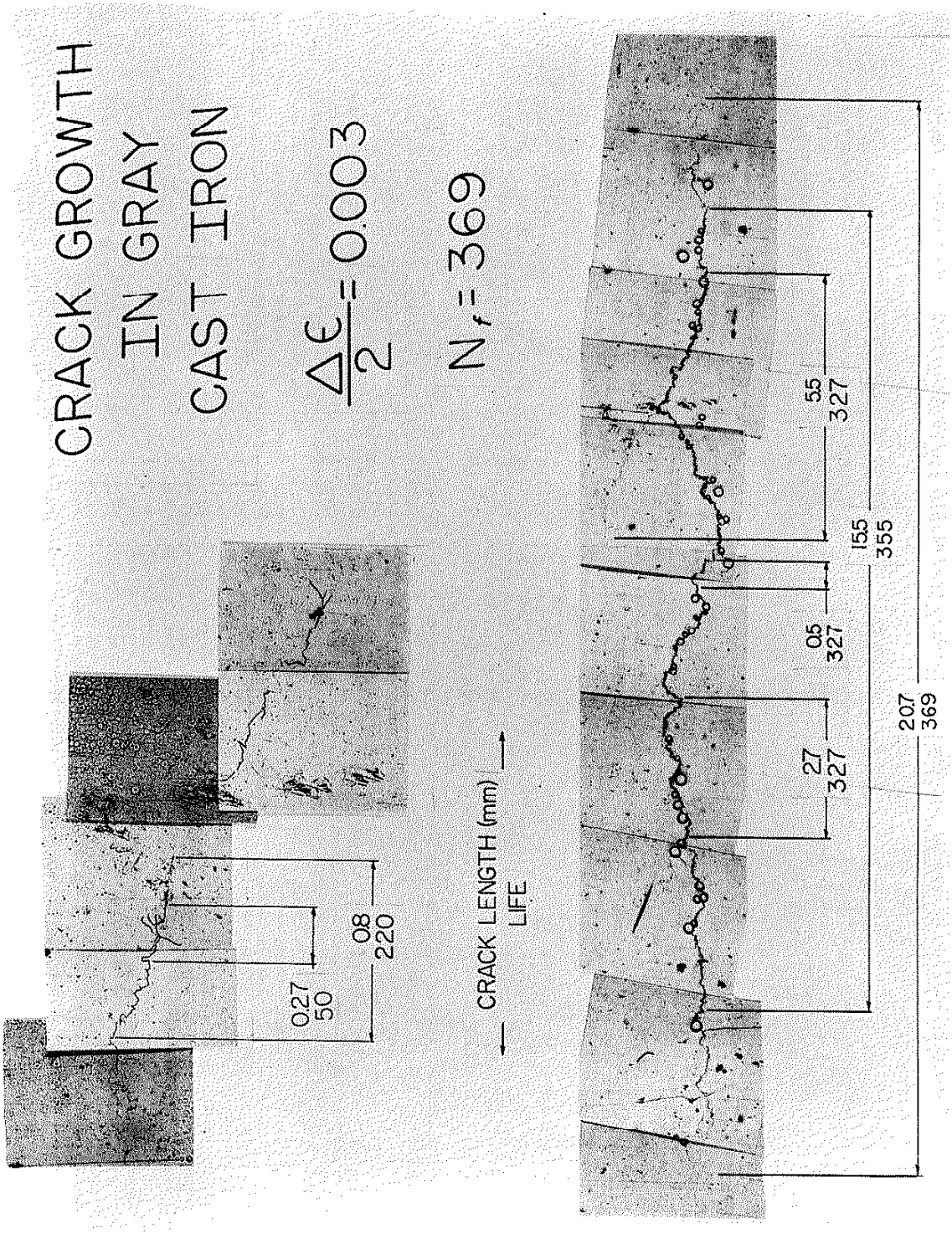

FIG. B3 CRACK DEVELOPMENT IN PEARLITIC IRON; $\Delta\varepsilon/2 = 0.003$.